NASA TECHNICAL NOTE

NASA TN D-4072

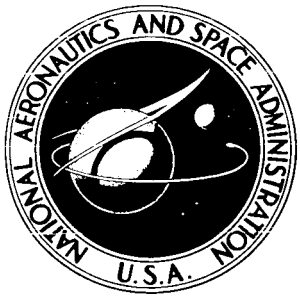

NASA TN D-4072

GEOMETRIC EFFICIENCY OF AN ELECTROFORMED NICKEL SOLAR CONCENTRATOR

by Conrad M. Willis and O. Karl Houck

Langley Research Center

Langley Station, Hampton, Va.

NATIONAL AERONAUTICS AND SPACE ADMINISTRATION • WASHINGTON, D. C. • AUGUST 1967

NASA TN D-4072

GEOMETRIC EFFICIENCY OF AN ELECTROFORMED NICKEL SOLAR CONCENTRATOR

By Conrad M. Willis and O. Karl Houck

Langley Research Center
Langley Station, Hampton, Va.

NATIONAL AERONAUTICS AND SPACE ADMINISTRATION

For sale by the Clearinghouse for Federal Scientific and Technical Information
Springfield, Virginia 22151 – CFSTI price $3.00

GEOMETRIC EFFICIENCY OF AN ELECTROFORMED NICKEL SOLAR CONCENTRATOR

By Conrad M. Willis and O. Karl Houck
Langley Research Center

SUMMARY

Geometric efficiency of a 152-centimeter-diameter paraboloidal solar-energy concentrator has been calculated from optical-ray-trace data. The data were obtained by reflecting a beam of light, which was parallel to the concentrator axis, from the concentrator to a focal-plane image plate and measuring image displacement from the concentrator axis. Two of the three methods used to calculate efficiency provided results that were within 0.025 of the measured calorimetric efficiency for energy-absorber apertures larger than $1\frac{3}{4}$ solar-image diameters. The data were also used to calculate the slope errors of the concentrator reflective surface. The values of one standard deviation of slope error were 1.45 milliradians for the radial component and 2.32 milliradians for the circumferential component.

INTRODUCTION

Solar-energy conversion systems utilizing solar concentrators are currently being considered for space-vehicle electrical power. The evaluation of system capabilities includes tests of concentrator efficiency to aid in matching the concentrator with a heat receiver. Concentrator efficiency, the ratio of solar energy reflected into a focal-plane aperture to the energy incident upon the concentrator, can be determined by two types of investigations. The most common method is to test in sunlight, by using a calorimeter, radiometer, or other heat receiver to measure the rate at which energy is collected for a range of receiver aperture sizes and locations. (See refs. 1 to 4.) This method provides a direct measurement of efficiency but requires the use of an elaborate test fixture to maintain continuous alinement of the optical axis with the solar rays. In the second type of investigation, light rays reflected from the concentrator are intercepted and traced to the known location of the light source. This ray-trace information defines the surface geometry and, if surface reflectance is known, concentrator efficiency can be calculated (ref. 5). Although ray-trace techniques have not been used widely for efficiency calculations, they do offer some advantages over calorimetric tests. Ray-trace tests permit measurement of location and extent of slope errors and thus aid in selection of

improved techniques for concentrator fabrication. In addition, ray tracing requires less elaborate facilities than calorimetric tests and can be performed in a controlled indoor environment that eliminates interruptions caused by unfavorable weather.

Most of the test techniques for obtaining ray-trace data use either a fixed light at the concentrator focus (refs. 6 and 7) or a ray parallel to the optical axis that can be directed at various concentrator locations (refs. 8 to 10). The latter method was used in the present investigation.

The solar concentrator evaluated was an electroformed nickel paraboloid 152 centimeters in diameter. Test data were obtained at about 700 regularly spaced locations on the concentrator surface. These data were used to calculate concentrator performance by a number of methods and were also used to calculate the slope error of the reflective surface. The accuracy of the efficiency calculations was determined by comparisons with the experimental values of efficiency reported in reference 1 for calorimetric tests of the same concentrator in sunlight.

SYMBOLS

d	displacement of image from concentrator axis, $\sqrt{x^2 + y^2}$, centimeters
D	concentrator diameter, 152 cm
f	focal length experimentally selected for concentrator, 65.5 centimeters
h	distance from focal plane to reflective surface, $h = -z = f - r^2/4f$, centimeters
i,j,k	orthogonal coordinate system (see fig. 14)
R_a	radius of heat-receiver aperture, centimeters
R_i	radius of solar image, $f \tan \alpha$, 0.305 centimeter
R_s	radius of solar concentrator, 76 centimeters
r	test radius, measured from collimated light to concentrator axis, centimeters
S	projected area of solar concentrator, centimeters^2
s	partial area assigned to set of test data, centimeters^2
x,y,z	rectangular Cartesian coordinates with origin at concentrator focal point; x and y define location of focal-plane images, and z defines axial location of assumed paraboloidal reflective surface, centimeters (see fig. 1)

x'', y'' circumferential and radial slope error, respectively, from reference 5 (see appendix)

α half-angle subtended by sun, 4.6 milliradians

δ_c circumferential slope error of reflective surface, angle between traces of tangent planes of concentrator and ideal paraboloid in focal plane, $\tan^{-1} - \frac{x}{(r - y)}$, milliradians (see fig. 2)

δ_r radial slope error of reflective surface, difference in angles between focal plane and tangent planes of concentrator and ideal paraboloid, $\tan^{-1} \frac{r}{2f} - \frac{1}{2} \tan^{-1} \frac{\sqrt{(r - y)^2 + x^2}}{h}$, milliradians (see fig. 2)

η_g geometric efficiency, ratio of energy entering given size of focal-plane aperture to total energy that is specularly reflected from concentrator

η_l local efficiency, calculated from data for single test radius

θ_p angle between incident and reflected rays for paraboloid, radians

θ_s angle between incident and reflected rays for solar concentrator, $\theta_p - 2\delta_r$, radians

σ standard deviation of slope errors from mean error, $\left[\frac{\Sigma\delta^2 - \frac{1}{N}(\Sigma\delta)^2}{N - 1}\right]^{1/2}$ where N is number of data points used and δ represents either δ_r or δ_c

ϕ azimuth angle used to locate points on concentrator, radians (see fig. 1)

MODEL

The solar concentrator investigated is a 152-cm-diameter, $\frac{\pi}{3}$-radian-rim-angle, electroformed nickel paraboloid. (See fig. 3.) The concentrator shell is supported at the rim by a rear-mounted torus that is attached with an electroformed transition strip. The front face of the shell is coated with a film of vacuum-deposited aluminum for higher solar reflectance. A more detailed description of the model is given in references 1 and 3.

APPARATUS AND PROCEDURE

A sketch and a photograph of the optical test apparatus are shown in figures 4 and 5, respectively. The primary parts are a light collimator, a focal-plane image plate, and a turntable for mounting the concentrator. The light source for the collimator was a 2-watt tungsten arc lamp having an 0.18-mm-diameter source. The source was at the focus of a 19.2-cm-focal-length objective lens. An adjustable aperture in front of the lens was used to control the diameter of the light beam incident on the concentrator. Beam diameter was varied from about 2 mm at the inner test radius to 7 mm at the rim to provide a legible image. During testing a ray of collimated light, directed parallel to the optical axis, was reflected from the concentrator to the ground-glass image plate and the image locations were recorded by a remotely controlled 35-mm camera. Some typical images are shown in figure 6. The light was directed at the desired test area by sliding the light along a radial track and rotating the concentrator about the optical axis. (See fig. 4.) An electric motor, controlled by a cam on the turntable axle, was used to rotate the concentrator through preset angles. The room in which the concentrator was tested was darkened to increase image visibility and a sufficiently constant temperature was maintained to eliminate thermal stress changes.

Before mounting the concentrator on the turntable, the turntable axis was adjusted to a vertical position by using a precision level. The collimator was then adjusted until a ray of light was reflected back to its source by a carefully leveled plane mirror. This procedure alined the ray parallel to the turntable axis of rotation. The concentrator was then mounted on the test fixture with the vertex approximately on the turntable axis. The test focal-length setting for the image plate was selected by determining the setting that produced minimum variation in the radial component of image displacement with radial position of the collimated light. The difference between experimental settings selected by ray-trace and calorimetric methods (ref. 1) was less than the estimated measurement accuracy.

Angular alinement of the concentrator optical axis with the turntable axis of rotation was accomplished by axial displacements of the mounting brackets at the concentrator rim. The optimum angle was selected for minimum variation in the radial component of image displacement with turntable rotation.

Data were obtained for test areas located at angular intervals of $\pi/45$ radians for eight equal annular areas into which the concentrator was divided. The seven inner test radii were selected by subdividing each annulus into two equal areas. A preliminary survey of the outermost annulus indicated that the change in slope error with radial location was too rapid for adequate representation of the area by a single test radius. Therefore, the 90 test locations assigned to this annulus were divided among 4 test radii. The actual locations used are indicated in table 1.

DATA REDUCTION AND ANALYSIS

The focal-plane image locations (fig. 6) on the photographic film were measured with respect to backlighted scales at the edge of the image plate. These measurements, in the form of x and y coordinates, were punched into cards by use of a semiautomatic film-reading machine. A computer program was then used to make adjustments to the data and to calculate concentrator efficiency and slope errors.

Compensation for Experimental Error

Two operations were performed on the data that partially compensate for the experimental error in alining the light source and concentrator axis with the axis of rotation. If the concentrator optical axis is not parallel to the turntable axis, rotation of the concentrator will produce a sinusoidal variation in the x and y components of image displacement. There will be a $\pi/2$ phase difference between x and y, the period will be equal to one rotation of the concentrator, and the amplitude will be determined by the misalinement angle of the concentrator and the test radius of the collimated light. Note that lateral displacement of the concentrator axis from the axis of rotation also produces a similar effect. However, the amplitude of the error is equal to the lateral displacement and thus is independent of test radius. Separation of these two effects was difficult and all the error was assigned to angular misalinement. The amplitude and phase of this misalinement were calculated by fitting a sine wave to the data. The calculated angle of 0.47 milliradian is about 0.05 of the angle subtended by the sun. All test data were corrected by displacements corresponding to the calculated angle at the respective test radius.

The second correction consisted of a mathematical translation of the coordinate system origin from the lighted grid at the edge of the image plate to a best focal-point location. The selected location approximates the optimum position for the center of a heat-absorber aperture and partially compensates for experimental error in alinement of the light source with the concentrator axis. The Y-axis was adjusted for each test radius so that the average value of circumferential error for that radius would equal zero. Each of the images was then mathematically rotated through the appropriate concentrator azimuth angle ϕ about the turntable axis. This rotation placed the images in the position they would occupy with a solar source. The X-axis was then located so that it passed through the geometric center of the image pattern from the complete concentrator, and the images were then returned to the location occupied before rotation. The translated origin location was assumed to lie on the concentrator axis and the image displacements were measured with respect to this point.

The corrected values for image displacement from the concentrator axis were then used to calculate concentrator characteristics.

Geometric Efficiency

Geometric efficiency, or the ratio of solar energy entering an aperture of a given radius to the total amount of specularly reflected energy, was calculated from ray-trace data by three methods: image count, uniform image, and random error.

Image count method.- The simplest procedure used to estimate geometric efficiency was the image count method. This consisted of counting the number of image centers falling inside a circular aperture and determining the ratio of this number to the total number of images. Since the images represent equal concentrator areas, the ratio is proportional to the energy entering the aperture.

Uniform image method.- The uniform image method uses two simplifying assumptions regarding the shape and energy distribution of the solar image: (1) a circular shape with a diameter equal to the minor axis of the actual elliptical image and (2) a uniform energy distribution across the assumed diameter. This diameter assumption was considered a reasonable compromise between image area and energy distribution since the solar image has a low intensity near the edge. The image area lying inside apertures of various sizes was calculated for each test point and the ratio of these areas to the total image area was considered to be the geometric efficiency.

Random error method.- For the random error method, the mathematical model described in reference 5 was used. Concentrator slope errors were assumed to have a random distribution in setting up the model; therefore, the ratio of concentrator focal length to diameter and the standard deviation of the measured slope error were the only data required to calculate efficiency. The error angles used in this method (projected-normal system) are defined and compared with a normal distribution in the appendix.

Slope Errors

In addition to calculating efficiency, the focal-plane images were also used to calculate slope errors of the reflective surface. As is the usual practice, all image displacement was assumed to result from a rotation of the reflective surface and the accompanying displacement of the concentrator surface from the ideal paraboloid was neglected. Therefore, the calculated slope errors do not represent the actual concentrator imperfections but an equivalent set of errors that will produce the given focal-plane-image distribution.

The slope errors were broken down into two components to facilitate analysis. The radial component, δ_r, moves the intersection of the reflected ray with the optical axis away from the focal plane and the circumferential component δ_c displaces the ray from the optical axis. The formulas used to calculate the angles are shown in the symbol list and sketches illustrating the angles are presented in figure 2. This system does not follow the convention, commonly used in optical work, of defining the tangent plane by the

angles between the ideal surface normal and projections of the actual normal on two mutually perpendicular planes containing the ideal normal. However, the system used herein does have the advantage of giving physical angles through which the tangent plane is rotated and the angles are not coupled (i.e., the same orientation of the tangent plane is described regardless of whether the δ_c or δ_r rotation is performed first).

Accuracy

Image coordinates were measured to an accuracy of ±0.02 cm based on the agreement between repeated data points. This represented an error that varied from 0.06 to 0.14 milliradian for the radial component and 0.26 to 1.00 milliradian for the circumferential component, with the maximum error occurring at the innermost test radius. Since this measurement error was random, the effect on efficiency should be small because of the large number of data points considered.

Two separate types of error were involved in image-plate location: (1) setting the image plate at the optimum position selected by observation of image distribution patterns and (2) measurement of the distance from the image plate to concentrator vertex. The plate was set at a position within ±0.04 cm of the optimum focal distance and the set distance was measured to within ±0.2 cm. The ±0.04-cm error in image-plate location produces an error in image location that varies from ±0.07 cm for images reflected from the rim to 0 for vertex images. The ±0.2-cm error in focal-length measurement is only 0.3 percent of the focal length and has a negligible effect on the calculation of slope error and efficiency.

RESULTS AND DISCUSSION

The basic data for this investigation were measurements locating the focal-plane images formed by the reflection of light rays, directed parallel to the optical axis, from various areas of the concentrator. These data, after reduction, show the distribution of images in the focal plane and are analyzed to obtain the magnitude of imperfections in geometry of the reflective surface and geometric efficiency of the concentrator.

Focal-Plane-Image Distributions

Examples of image locations in the form of x and y components of displacements from the optical axis are presented in figure 7. The general level of the y, or radial, component decreases with increasing test radius, indicating a decrease in the local focal length of the annular area being surveyed. The root-mean-square value of all image displacements d was found to be $1.59R_i$ where $d = \sqrt{x^2 + y^2}$.

Comparison of Calculated Efficiency With Calorimetric Data

The geometric efficiency of the concentrator was calculated by the three methods previously described and was compared with values obtained from calorimetric tests (ref. 1) to indicate the relative accuracy of the various methods. Calorimetric efficiency was converted to geometric efficiency by dividing by the specular reflectance of the concentrator surface. Since the calorimetric-efficiency curve of reference 1 was nearly flat at large apertures and reradiation losses from the cold calorimeter were small, the specular reflectance was assumed to be equal to the 0.865 efficiency measured at the largest aperture ($R_a = 8.3\ R_i$).

The variation in geometric efficiency with aperture size (as obtained from calorimetric data) is shown in figure 8(a) to establish concentrator quality. Figure 8(b) shows the difference between the geometric efficiencies obtained from calorimetric data and those calculated for a range of aperture sizes. Both the image count and the uniform image methods gave calculated efficiencies that were within 0.025 of the measured values for aperture diameters larger than $1\frac{3}{4}$ solar-image diameters. Solar-power conversion devices currently being developed provide the highest system efficiency in the range from $1\frac{3}{4}R_i$ to $7R_i$. For the present concentrator, aperture sizes below this range are of little interest because of the low concentrator efficiency at small apertures (fig. 8(a)), and at aperture sizes above this range the cavity temperatures obtained are too low for efficient conversion. The erroneously high efficiency indicated by the random error method for aperture radii near $3R_i$ in figure 8(b) is probably due to the departure of test data from the assumed random distribution of slope errors (see appendix).

All methods gave good results at aperture radii larger than 5 solar-image radii. Good accuracy could be expected in this range because the geometric efficiency is approaching 1.0 as shown in figure 8(a). Since only a small percentage of the images are not completely enclosed by the aperture, the error in calculating the energy loss due to areas falling outside the aperture will also be a small part of the total.

Variation in Local Efficiency With Concentrator Radius

The efficiency data previously shown were calculated by averaging the local values of efficiency at many concentrator locations. This average value is all that is needed to specify the performance of a given configuration. However, the local values do vary considerably with radial location and the local efficiency of a given area is of interest if configuration changes (e.g., changing from a rear- to front-mounted support torus) are to be considered.

The variation in local geometric efficiency with radial location of the annular test area is presented in figure 9 for three aperture sizes. The efficiencies were calculated by the uniform image method because it was believed that this method might be more

reliable than image counting for the limited number of data points available. An aperture radius of 2 solar-image radii was large enough to completely enclose all images from locations inboard of $r/R_S = 0.8$. A rapid decrease in efficiency occurred with increasing radius for the outer portion of the concentrator. This decrease was mainly due to an increase in image displacement (see fig. 7) but was aggravated by the increasing image size. With an aperture radius of 1.25 solar-image radii, there were some image displacements at all radial test stations that were large enough to place the assumed circular image partially outside the aperture and thus lower the efficiency.

Reflective-Surface Slope Errors

Slope error, or the rotation of the paraboloid surface that would produce the measured focal-plane-image displacement from the optical axis, was calculated for each test point. This rotation was broken down into radial and circumferential components for convenience of analysis. A complete tabulation of the slope-error data is presented in table 1.

Surface slope errors for three radial locations on the concentrator are presented in figure 10. The peak-to-peak variation of circumferential error was higher than that of the radial component. Some of the areas having high slope errors (such as the regions around $\phi = 1.9\pi$) appear to be long narrow areas extending across more than one test radius.

Figure 11 presents the average and root-mean-square value of radial and circumferential slope error at each test radius. The average circumferential slope error is zero because the trace of the concentrator forms a closed figure on the plane in which the angle is measured. The rapid change in average radial error outboard of $r/R_S = 0.8$ causes a corresponding change in local focal length or distance at which rays from a given test radius intersect the optical axis. This increased local focal length or roll-off is probably due to stresses introduced at the shell-torus junction.

Both components of error have root-mean-square (rms) minimums at intermediate values of concentrator radius. The radial error rms minimum occurs at an intermediate radius because the focal length in this region is about equal to the average focal length or distance at which the image plate was set. Circumferential error is independent of image-plate setting and the rms minimum probably represents the point of best surface geometry. However, the rms values are influenced slightly by the decreasing accuracy of measurement with decreasing test radius. One standard deviation of slope error was 1.45 and 2.32 milliradians for the radial and circumferential components, respectively.

The fraction of concentrator area having less than a specified value of slope error is shown in figure 12. This figure shows the circumferential error to be greater than radial error for any amount of area considered. It should be pointed out, however, that

radial error is more detrimental to efficiency because a given radial error will produce an image displacement that is larger than that produced by the same angle of circumferential error. The variation in image displacement with radial location of the error is shown in figure 13. The displacement due to a given slope error varies from 0 for a circumferential error at the concentrator vertex to nearly 1.2 solar-image radii per milliradian for a radial error at the concentrator rim. Displacements due to circumferential error are proportional to the distance from the optical axis and are much smaller than those produced by an equal radial error.

CONCLUDING REMARKS

Optical-ray-trace data obtained from a 152-centimeter-diameter paraboloidal solar concentrator have been used to calculate geometric efficiency and surface slope errors. Two of the methods used to calculate efficiency gave results that were within 0.025 of experimental values for energy-absorber aperture diameters larger than $1\frac{3}{4}$ solar-image diameters. It is, therefore, concluded that geometric efficiency can be calculated with reasonable accuracy for paraboloidal concentrators having surface errors that are the size of those for the test concentrator. The concentrator had a root-mean-square value of image displacement equal to 1.59 solar-image radii. The value of one standard deviation of slope error was 1.45 milliradians for the radial error and 2.32 milliradians for the circumferential error.

The concentrator area having the best geometry was about midway between the rim and vertex. The area of poorest geometry was adjacent to the support torus at the rim.

Langley Research Center,
National Aeronautics and Space Administration,
Langley Station, Hampton, Va., March 1, 1967,
120-33-06-08-23.

APPENDIX

Comparison of Slope Error With a Random Distribution

One of the basic requirements for accurate calculation of concentrator efficiency by the random error method is that the slope errors approximate a random distribution. The mathematical model of reference 5 used for this method defines slope-error angles that are not identical to the angles used in the present paper. The angles used in reference 5 will be referred to as projected-normal angles to distinguish them from the rotated-tangent angles defined in the symbol list of this paper.

A sketch defining the projected-normal slope error is presented in figure 14. The origin O of the i,j,k orthogonal coordinate system is placed at the point where the incident ray of light strikes the reflective surface. The k-axis is coincident with the surface normal of the assumed paraboloid and the j-axis intersects the optical axis. The concentrator surface normal $\overline{OA}$ is projected on the ik- and jk-planes to produce vectors $\overline{OB}$ and $\overline{OC}$, respectively. Circumferential slope error x'' and radial slope error y'' are the angles between the paraboloid surface normal and the projections of concentrator surface normal on the planes shown. Since all concentrator errors considered will be small, reference 5 assumes that the angle is equal to the tangent of the angle shown in figure 14.

Angles measured in the rotated-tangents system (δ_c and δ_r) used in the text are related to the projected-normal angles (x'' and y'') used in reference 5 by the following formulas:

$$x'' = \tan \delta_c \frac{\sin\left(\frac{\theta_p}{2} + \beta\right)}{\cos \beta}$$

$$y'' = \tan \beta$$

where

$$\frac{\theta_p}{2} = \tan^{-1} \frac{r}{2f}$$

and

$$\beta = \tan^{-1}\left[\cos \delta_c \tan\left(\frac{\theta_p}{2} + \delta_r\right)\right] - \frac{\theta_p}{2}$$

Angles measured by the two methods are the same for the case of pure radial error. The projected-normal slope errors are compared with a random distribution in figures 15 and 16. Error distributions for the individual test radii (fig. 15) appear to be a reasonable approximation of the straight line which represents a random distribution. However, the mean error varied with radial station and, consequently, the distribution of the data about the mean for the entire concentrator (fig. 16) showed considerably more departure from the random than was observed for individual test radii.

REFERENCES

1. Willis, Conrad M.: Calorimetric Evaluation of a 60-Inch (152-Centimeter) Electroformed Nickel Solar Concentrator. NASA TN D-3012, 1965.

2. Sweetnam, G. E.: Power Sources. Supporting Research and Advanced Development. Space Programs Summary No. 37-19, Volume IV (Contract No. NAS 7-100), Jet Propulsion Lab., California Inst. Technol., Feb. 28, 1963, pp. 47-55.

3. Pichel, M. A.: Research and Development Techniques for Fabrication of Solar Concentrators. Rept. 1587-Final (Contract NAS 7-10), Electro-Opt. Syst., Inc., Dec. 27, 1961.

4. Schwartz, S.; and Bagby, J.: Rigidized Inflatable Solar Energy Concentrators. NASA CR-254, 1965.

5. Schrenk, G. L.; and Gritton, D. G.: Analysis of Solar Reflectors – Mathematical Theory and Methodology for Simulation of Real Reflectors. EDR 3693 (Contract AF04(695)-335), Allison Div., Gen. Motors Corp., Dec. 16, 1963. (Available from DDC as AD 602 870.)

6. Castle, Charles H.: Final Report – Fabrication of a 60 Inch Diameter Stretch Formed Aluminum Solar Concentrator. ER-5058, Thompson Ramo Wooldridge Inc., Sept. 14, 1962.

7. Anon.: Optical System for Inspection of Parabolic Mirrors. Final Report Appendices – Solar Thermionic Electrical Power System. ASD Tech. Rept. 1961, U.S. Air Force, Dec. 1961, pp. G-1 – G-46.

8. Sanborn, D. S.: The Development of Deployable Solar Concentrators for Space Power. Paper presented at 1961 SAE National Aerospace Engineering and Manufacturing Meeting (Los Angeles, Calif.), Oct. 9-13, 1961.

9. Tanenhaus, Abraham M.: Inflated-Rigidized Paraboloidal Solar Energy Concentrator Evaluation. GER-10295, Goodyear Aircraft Corp., July 20, 1961.

10. Rouklove, Peter; and Blake, Floyd A.: Performance Testing of a Solar Electrical Thermionic Generator System. Jet Propulsion Laboratory paper presented at the Solar Energy Society Conference (Phoenix, Ariz.), Mar. 15-17, 1965.

TABLE I.— SLOPE ERROR OF REFLECTIVE SURFACE

Azimuth ϕ radians	Circumferential error, δ_c, radians — Radius r/R_s										
	0.250	0.433	0.559	0.661	0.750	0.829	0.902	0.968	0.977	0.980	0.986
0 $\frac{2\pi}{90}$	-43.$\times10^{-5}$	106.$\times10^{-5}$	8.$\times10^{-5}$	-84.$\times10^{-5}$	-77.$\times10^{-5}$	-167.$\times10^{-5}$		-257.$\times10^{-5}$			
1	272.	41.	-15.	-58.	-93.	-128.					
2	342.	-57.	70.	-98.	-108.	-176.		-217.			
3	114.	53.	22.	-25.	-103.	-135.					
4	363.	-77.	55.	-87.	-37.	-76.	-124.$\times10^{-5}$	-128.			
5	139.	-69.	10.	-57.	-30.	-51.	-100.				
6	272.	9.	-9.	-27.	-42.	-60.	-108.	-215.		-375.$\times10^{-5}$	2229.$\times10^{-5}$
7	-127.	-49.	27.	-18.	6.	-52.	-67.				
8	67.	-4.	-17.	36.	-4.	-7.	-9.	31.			
9	438.	-61.	-33.	46.	6.	39.	82.				
10	282.	-15.	58.	34.	36.	32.	29.	161.			
11	64.	-105.	42.	22.	27.	-11.	-104.				
12	-92.	253.	1.	78.	38.	1.	-76.	-147.	-164.$\times10^{-5}$	-337.	
13	-76.	-9.	-13.	23.	11.	31.	-47.				-3294.
14	-107.	-29.	-134.	57.	82.	114.	126.	226.			
15	151.	-14.	92.	25.	55.	163.	172.				57.
16	115.	-33.	-1.	-53.	28.	51.	187.	478.			
17	-97.	16.	-40.	73.	279.	226.	461.				969.
18	44.	32.	26.	41.	14.	-29.	-288.	-564.		-522.	
19	-110.	13.	-13.	-37.	-12.	-335.	-452.				-518.
20	33.	-6.	0.	-24.	-158.	-109.	-405.	-649.	-574.		
21	115.	-60.	14.	12.	-6.	-166.	-324.				
22	20.	-79.	54.	-66.	-33.	-47.	-181.	-243.			
23	-16.	-134.	-66.	-98.	-100.	-34.	-40.				
24	-111.	-50.	-133.	-131.	-48.	31.	102.	191.			
25	-31.	-105.	-94.	-51.	-55.	-27.	34.				
26	49.	-22.	-55.	-62.	-64.	-68.	-66.	246.			97.
27	-284.	-112.	-96.	-51.	-72.	-110.	-231.				
28	148.	-65.	-112.	-40.	-62.	-117.	-202.	-309.			-343.
29	-11.	-53.	32.	-53.	-51.	-54.	-47.				
30	-170.	-111.	-65.	-43.	-101.	27.	27.	173.		261.	193.
31	0.	-100.	-82.	-57.	-13.	18.	68.				
32	0.	-39.	-87.	-4.	-34.	-8.	-27.	-8.			166.
33	124.	-30.	-79.	26.	-7.	-36.	-51.				
34	-40.	-22.	34.	55.	59.	-29.	-92.	-111.	32.		-35.
35	88.	-15.	14.	61.	5.	-6.	-38.				
36	-138.	26.	-8.	44.	70.	17.	-32.	-69.		172.	104.
37	-13.	65.	77.	70.	74.	56.	-28.				
38	170.	0.	0.	96.	136.	165.	71.	134.			
39	175.	3.	83.	121.	178.	168.	249.				
40	-58.	-29.	31.	10.	-136.	205.	443.	453.			
41	-234.	-29.	-48.	-79.	240.	295.	640.				527.
42	-293.	-63.	-48.	101.	379.	385.	333.	393.	575.	563.	
43	-176.	-30.	84.	100.	101.	117.	331.				400.
44	55.	-33.	-25.	8.	218.	257.	281.	61.			
45	-185.	-105.	-55.	253.	274.	308.	-42.				
46	-134.	166.	48.	249.	251.	143.	-30.	142.			
47	-142.	57.	284.	244.	226.	156.	109.				
48	-35.	85.	91.	193.	241.	150.	184.	278.		274.	
49	-46.	112.	111.	142.	175.	144.	194.				246.
50	59.	172.	131.	180.		101.	90.	129.			
51	341.	129.	69.	127.		111.	65.				
52	266.	153.	114.	74.		85.	24.	67.			
53	189.	177.	157.	42.		111.	190.		265.		
54	112.	165.	40.	55.		65.	229.	313.		341.	
55	35.	153.	56.	-1.	62.	90.	73.				-103.
56	-221.	71.	-9.	56.	11.	-9.	109.	301.			
57	-124.	23.	6.	22.	20.	-56.	-80.				
58	267.	-60.	-34.	-80.	-230.	-263.	-255.	-563.			-354.
59	69.	-40.	-100.	-24.	16.	-81.	-202.				
60	105.	14.	-113.	-59.	-36.	-76.	-134.	-17.		8.	-62.
61	23.	-35.	-99.	-94.	-128.	-106.	-100.				
62	-237.	-50.	-139.	-152.	-102.	-137.	-49.	-47.			-314.
63	0.	-66.	-100.	-120.	-134.	-97.	-95.		-114.		
64	0.	-55.	-13.	-82.	-143.	-155.	-169.	-80.			
65	-100.	-71.	-54.	-163.	-195.	-221.	-279.				
66	-302.	-17.	-120.	-86.	-168.	-181.	-212.	-213.		-257.	
67	-323.	-33.	-27.	-121.	-142.	-141.	-177.				
68	67.	-47.	-14.	-133.	-75.	-83.	-111.	-63.			
69	-250.	-96.	-0.	12.	-68.	-8.	19.				
70	-96.	-7.	40.	-45.	-20.	-37.	6.	103.			
71	-57.	-21.	-25.	-34.	47.	57.	26.				
72	-137.	-0.	17.	-23.	56.	28.	46.	63.		65.	
73	-156.	56.	32.	11.	26.	87.	99.				
74	-56.	10.	75.	46.	75.	130.	168.	114.			
75	-14.	-2.	65.	82.	105.	156.	222.		165.		
76	-386.	22.	82.	51.	17.	111.	181.	303.			
77	-45.	47.	20.	-48.	9.	86.	140.				
78	119.	38.	39.	-10.	21.	-11.	20.	-89.		-203.	
79	-12.	-39.	-48.	-17.	-45.	-35.	-68.				
80	-82.	-11.	26.	-45.	-71.	-112.	-122.	-134.			
81	-209.	17.	-33.	-50.	-116.	-82.	-159.				
82	79.	-91.	-64.	-77.	-60.	-174.	-180.	-9.			
83	13.	77.	145.	145.	55.	-36.	73.		-182.		
84	-346.	383.	675.	413.	331.	652.	1037.	224.		14.	
85	183.	313.	-657.	-739.	-646.	-556.	-589.				
86	-54.	-511.	-205.	-63.	-29.	-112.	4.	-49.			
87	5.	-100.	8.	5.	-9.	-112.	-189.				
88	125.	4.	62.	-16.	-107.	-111.	-284.	-394.			
89	188.	75.	11.	-14.	-125.	-197.	-313.				
AVG	-4.	-0.	1.	-1.	-0.	-1.	-0.	0.	0.	0.	-2.
RMS	169.	106.	124.	124.	139.	158.	228.	256.	323.	309.	999.
SIGMA	170.	107.	125.	125.	140.	159.	229.	259.	345.	322.	1028.

TABLE 1. - CONCLUDED

Azimuth ϕ radians	Radial error, δ_r, radians: Radius r/R_s										
	0.250	0.433	0.559	0.661	0.750	0.829	0.902	0.968	0.977	0.980	0.986
0 $\frac{2\pi}{90}$	27.x10^{-5}	2.x10^{-5}	11.x10^{-5}	21.x10^{-5}	17.x10^{-5}	-52.x10^{-5}		142.x10^{-5}			
1	48.	27.	-11.	7.	38.	-43.					
2	127.	-19.	-1.	-2.	6.	-46.		89.			
3	43.	14.	-10.	12.	17.	-44.					
4	121.	-24.	-7.	-19.	-20.	-51.	-234.x10^{-5}	70.			
5	118.	16.	-10.	1.	-8.	-58.	-177.				
6	116.	13.	-19.	4.	-1.	-57.	-221.	-36.		424.x10^{-5}	242.x10^{-5}
7	32.	-4.	-8.	-4.	2.	-68.	-242.				
8	111.	-34.	-4.	5.	14.	-57.	-241.	197.			
9	28.	-15.	-19.	-9.	12.	-42.	-213.				
10	107.	12.	10.	1.	5.	-31.	-174.	359.			
11	24.	-26.	-4.	21.	23.	-37.	-187.				
12	22.	-13.	20.	3.	12.	-39.	-241.	68.	329.x10^{-5}	516.	
13	21.	14.	12.	24.	20.	-44.	-249.				449.
14	20.	-1.	30.	6.	49.	-50.	-277.	-11.			
15	19.	-9.	-34.	33.	48.	1.	-147.				384.
16	18.	-3.	3.	72.	67.	35.	-46.	-122.			
17	18.	-11.	-29.	15.	32.	138.	36.				-122.
18	17.	-11.	-23.	32.	57.	216.	6.	261.		55.	
19	99.	3.	-11.	15.	42.	-18.	25.				285.
20	99.	-18.	-36.	-24.	-3.	-69.	-32.	36.	179.		
21	18.	-18.	-16.	-41.	-17.	-73.	-223.				
22	19.	4.	-22.	-7.	-41.	-120.	-326.	38.			
23	19.	12.	-28.	-22.	-21.	-140.	-292.				
24	20.	-37.	-39.	-33.	-30.	-135.	-254.	-103.			
25	22.	-35.	-44.	-20.	-14.	-74.	-193.				
26	23.	-27.	-24.	-24.	-32.	-85.	-143.	-252.			278.
27	25.	-25.	-41.	-39.	-50.	-88.	-205.				
28	108.	-30.	-52.	-54.	-63.	-116.	-300.	-326.			284.
29	29.	-36.	-31.	-52.	-61.	-131.	-335.				
30	31.	-41.	-60.	-72.	-59.	-137.	-295.	-250.		166.	363.
31	0.	-38.	-58.	-53.	-71.	-122.	-248.				
32	0.	-23.	-57.	-55.	-82.	-123.	-238.	-258.			294.
33	14.	-42.	-48.	-52.	-70.	-137.	-258.				
34	16.	-32.	-39.	-88.	-77.	-143.	-289.	-135.	251.		680.
35	19.	-37.	-42.	-80.	-94.	-174.	-323.				
36	22.	-48.	-65.	-43.	-105.	-214.	-331.	-73.		436.	651.
37	25.	-59.	-36.	-68.	-117.	-228.	-384.				
38	28.	-63.	-65.	-82.	-153.	-199.	-425.	-109.			
39	31.	-24.	-36.	-73.	-111.	-162.	-400.				
40	35.	-64.	-27.	-64.	-98.	-180.	-367.	-97.			
41	38.	-32.	-49.	-78.	-45.	-36.	-182.				582.
42	41.	-15.	-52.	-47.	-47.	36.	-268.	-113.	293.	424.	
43	-37.	-47.	-49.	-44.	-9.	-30.	-294.				602.
44	47.	-59.	-65.	-18.	24.	4.	-328.	-97.			
45	-30.	-27.	-42.	24.	-8.	50.	-258.				
46	54.	-17.	-20.	22.	10.	-37.	-214.	-232.			
47	-24.	-21.	2.	19.	13.	-60.	-218.				
48	-21.	-46.	11.	-0.	16.	-74.	-204.	-311.		527.	
49	-19.	-29.	-5.	25.	9.	-63.	-164.				729.
50	-16.	-12.	42.	22.		-60.	-135.	-393.			
51	68.	-10.	38.	36.		-53.	-185.				
52	70.	-0.	72.	10.		-85.	-238.	-169.			
53	-9.	-5.	56.	35.		-57.	-221.		410.		
54	-7.	4.	-6.	31.		-55.	-167.	-270.		425.	
55	76.	6.	-10.	33.	33.	-23.	-123.				661.
56	78.	1.	4.	18.	55.	-30.	-110.	-454.			
57	80.	9.	6.	26.	66.	-20.	-3.				
58	0.	18.	14.	-12.	13.	-61.	10.	-481.			-4.
59	82.	5.	-4.	11.	-0.	-81.	-208.				
60	2.	-1.	3.	-10.	-29.	-63.	-248.	-287.		147.	435.
61	3.	28.	-9.	-9.	-43.	-80.	-221.				
62	84.	-29.	-21.	-20.	-23.	-109.	-213.	-145.			635.
63	0.	-14.	-27.	-31.	-18.	-83.	-216.		72.		
64	0.	-26.	-34.	-8.	-40.	-75.	-186.	-159.			
65	4.	-12.	-40.	-47.	-50.	-97.	-235.				
66	84.	-34.	-28.	-59.	-65.	-127.	-294.	-251.		319.	
67	3.	-6.	-41.	-43.	-71.	-115.	-328.				
68	83.	-50.	-36.	-44.	-77.	-154.	-344.	-301.			
69	1.	-22.	-56.	-61.	-78.	-147.	-312.				
70	80.	-31.	-32.	-63.	-79.	-152.	-324.	-252.			
71	-2.	-46.	-59.	-36.	-66.	-111.	-300.				
72	77.	-34.	-29.	-32.	-72.	-126.	-286.	-68.		714.	
73	75.	-28.	-31.	-34.	-40.	-115.	-285.				
74	73.	-2.	-20.	-19.	-37.	-99.	-268.	-167.			
75	-10.	-18.	-35.	1.	-14.	-54.	-218.		234.		
76	69.	-35.	-18.	10.	8.	-44.	-154.	-113.			
77	66.	-16.	-14.	2.	25.	-3.	-126.				
78	64.	-4.	-30.	27.	32.	-2.	-148.	-91.		281.	
79	61.	7.	-1.	46.	24.	8.	-139.				
80	58.	12.	3.	16.	41.	-16.	-161.	-21.			
81	55.	-6.	18.	41.	38.	-36.	-186.				
82	52.	-37.	9.	26.	-9.	-57.	-171.	73.			
83	49.	-5.	-7.	23.	37.	-12.	-110.		315.		
84	46.	-1.	-4.	42.	34.	31.	-66.	-83.		379.	
85	43.	61.	-14.	50.	70.	76.	-147.				
86	39.	-72.	-35.	36.	37.	73.	-120.	73.			
87	36.	-32.	25.	38.	44.	61.	-48.				
88	33.	1.	-4.	18.	16.	19.	-108.	76.			
89	30.	-2.	6.	26.	23.	-10.	-227.				
AVG	40.	-16.	-18.	-9.	-14.	-62.	-211.	-106.	260.	370.	413.
RMS	55.	28.	32.	38.	51.	95.	232.	207.	277.	408.	473.
SIGMA	38.	23.	27.	37.	49.	72.	98.	181.	103.	178.	238.

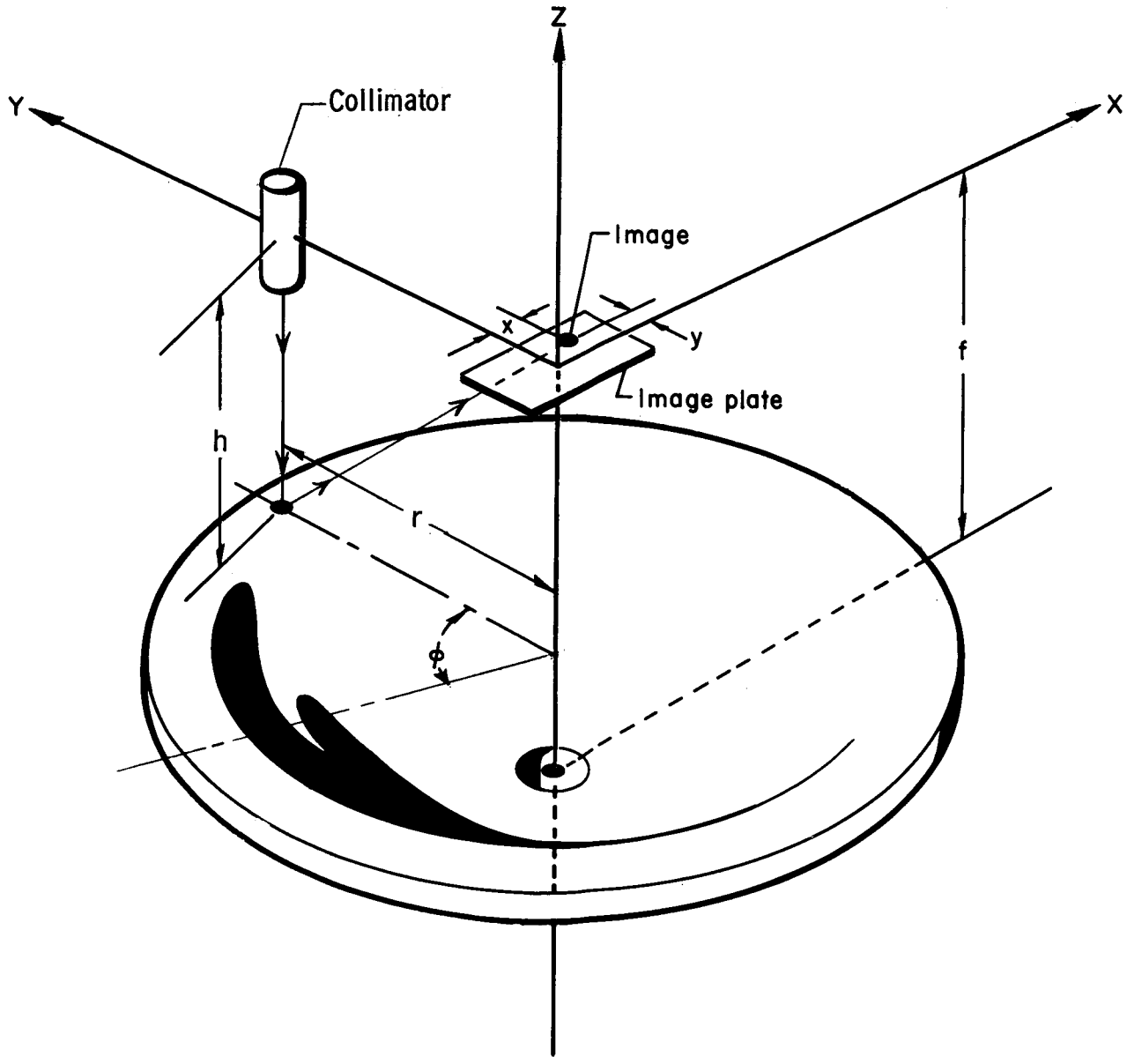

Figure 1.- Sketch defining coordinate system.

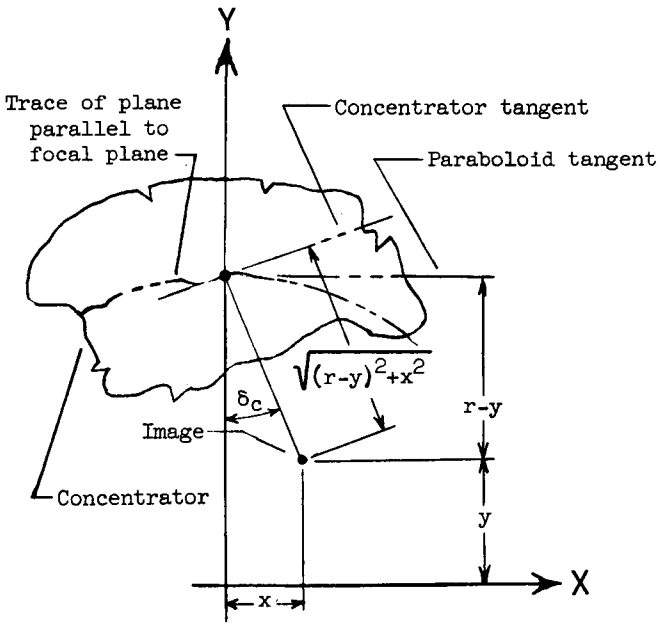

$$\delta_c = \tan^{-1} - \frac{x}{r - y}$$

(a) Circumferential error.

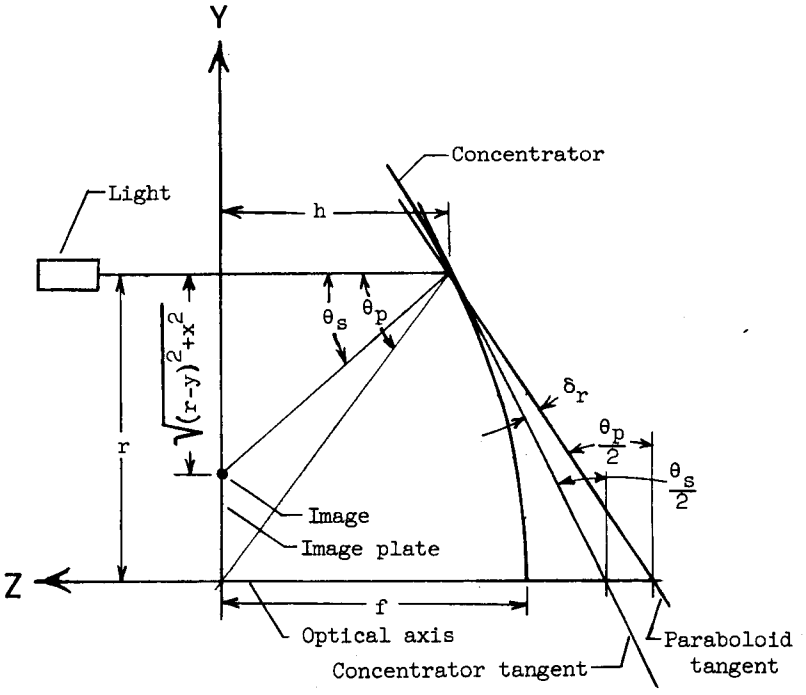

$$\delta_r = \frac{\theta_p}{2} - \frac{\theta_s}{2} = \tan^{-1} \frac{r}{2f} - \frac{1}{2} \tan^{-1} \frac{\sqrt{(r - y)^2 + x^2}}{h}$$

(b) Radial error. Angles have been rotated into YZ-plane for clarity.

Figure 2.- Sketches illustrating slope error.

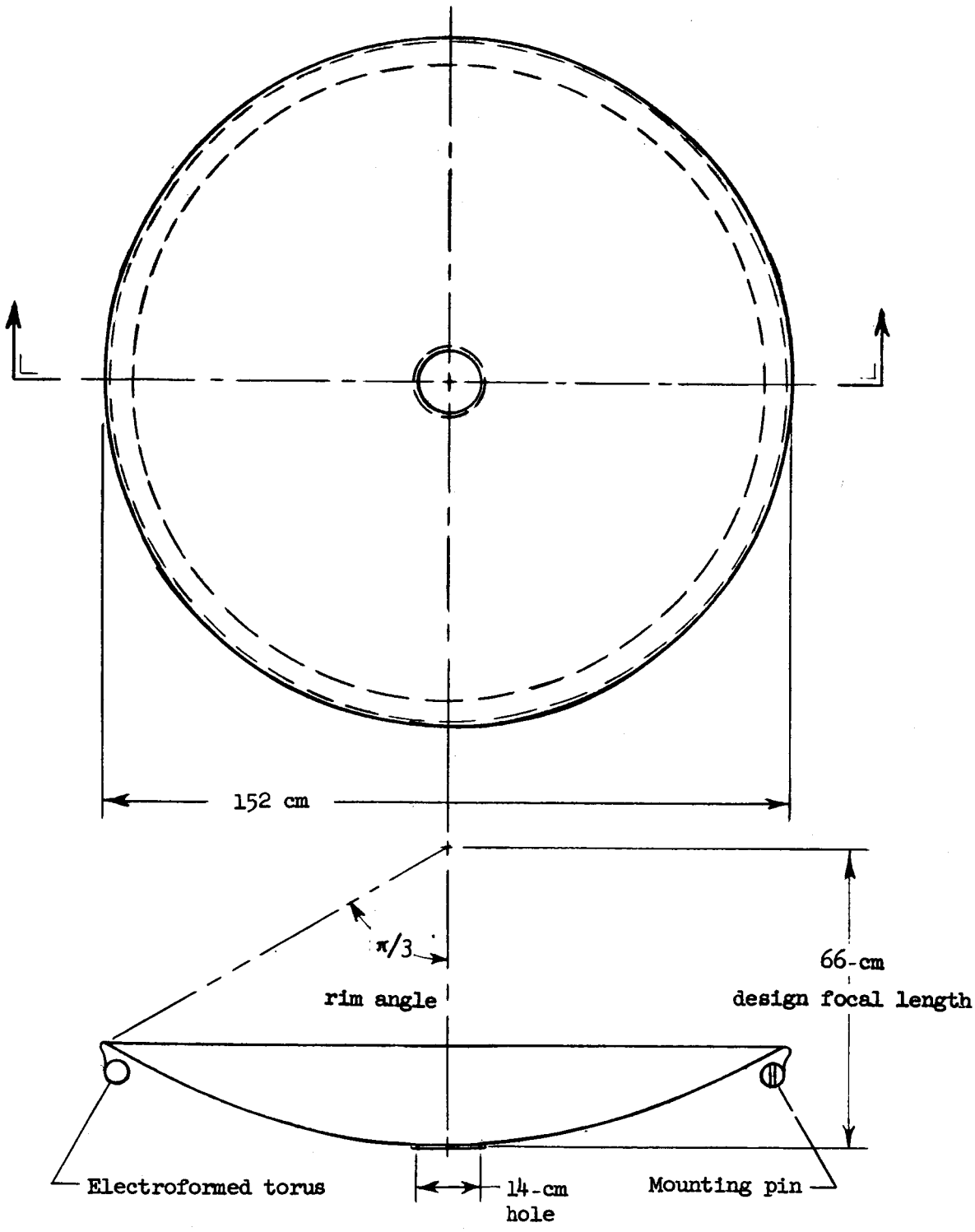

Figure 3.- Model geometry.

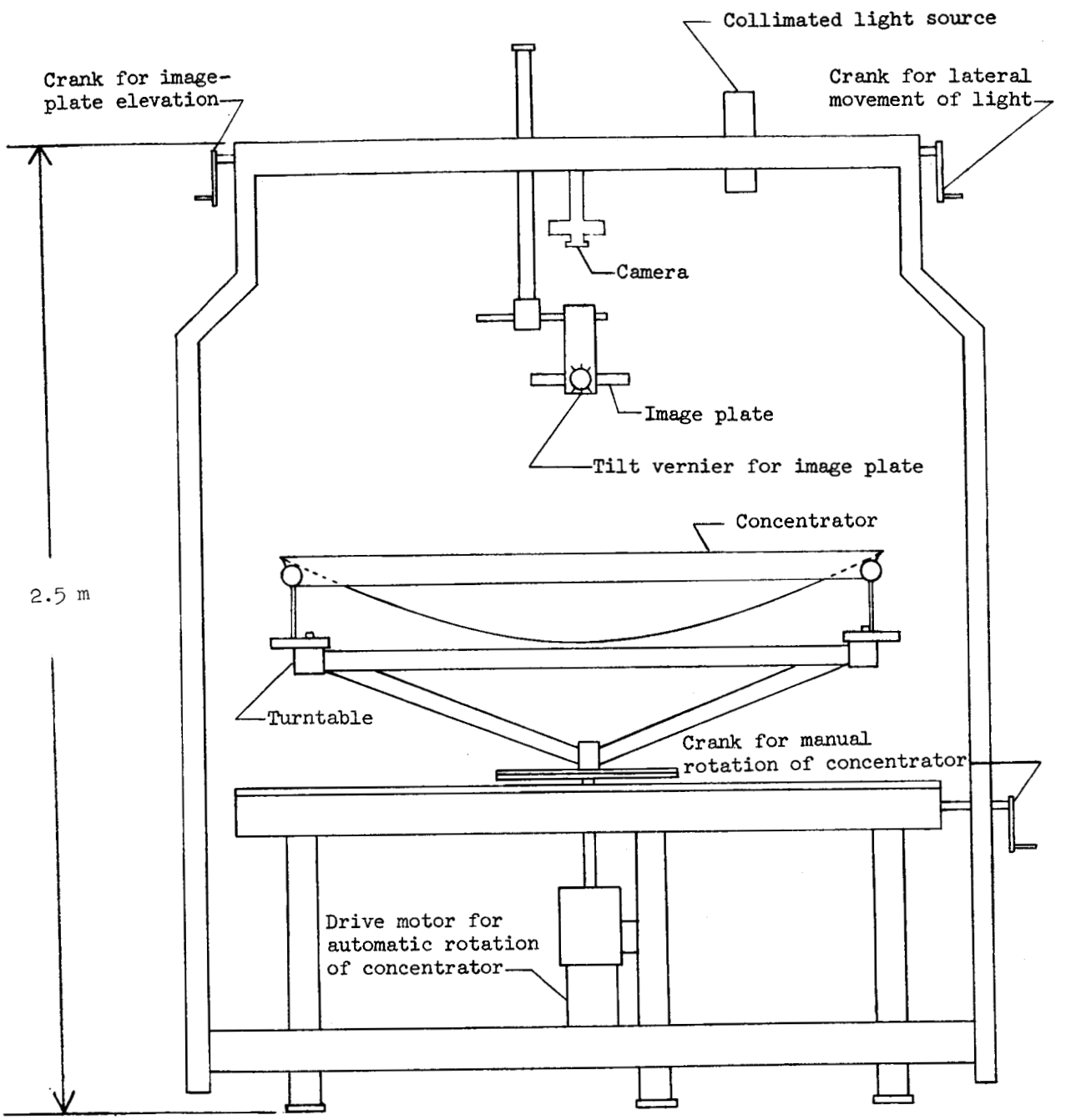

Figure 4.- Sketch of ray-trace test fixture.

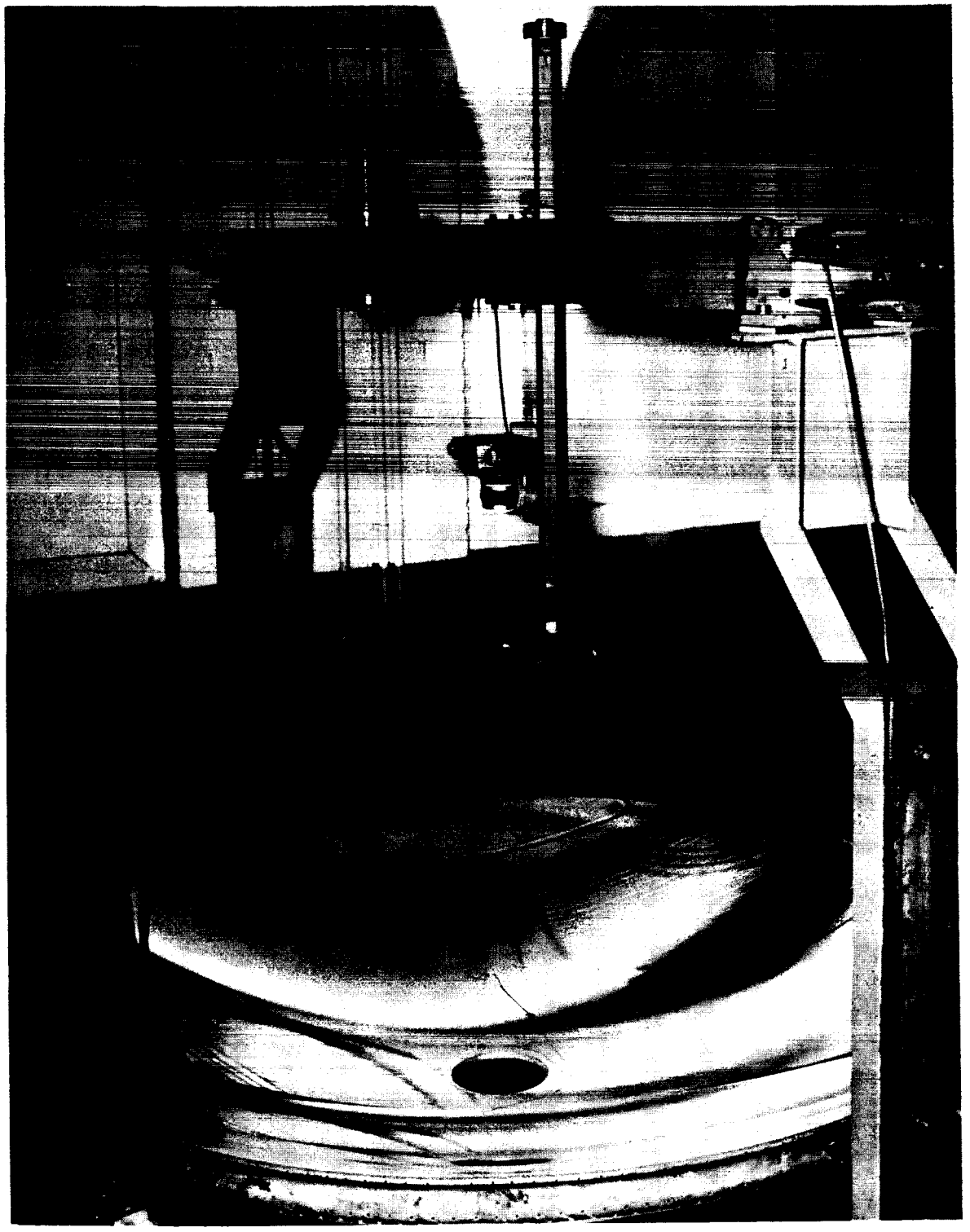

Figure 5.- Photograph of test fixture.

L-64-1913

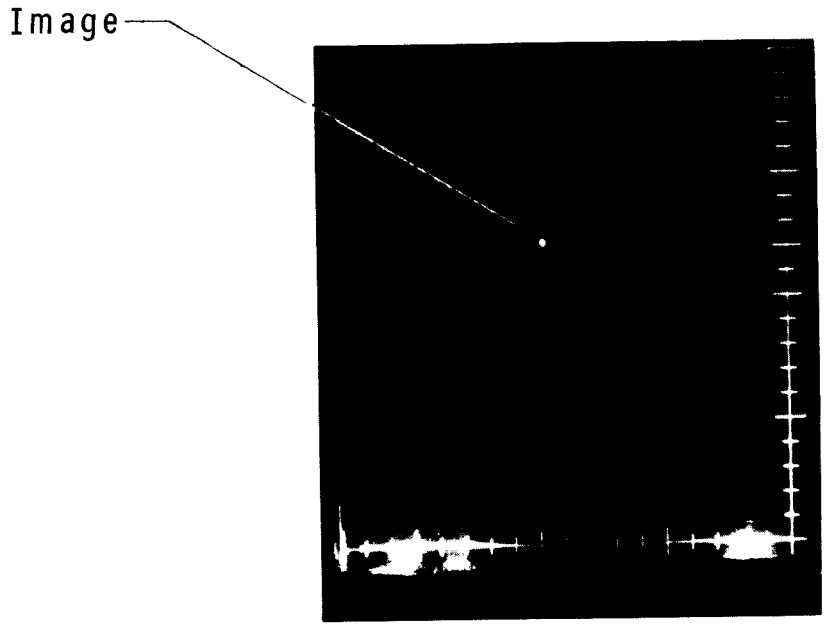

$r/R_s = 0.25$

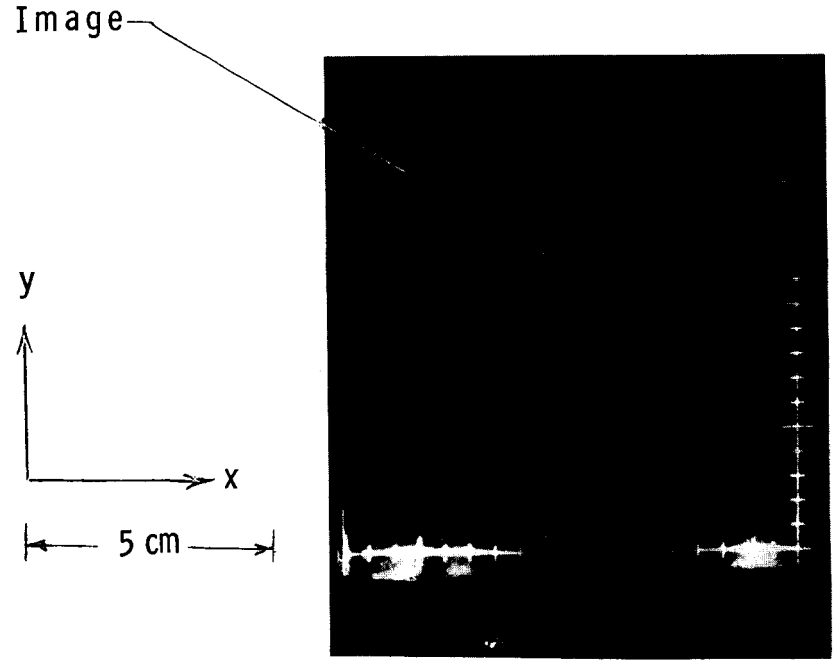

$r/R_s = 0.66$

Figure 6.- Sample image photographs.

L-67-1019

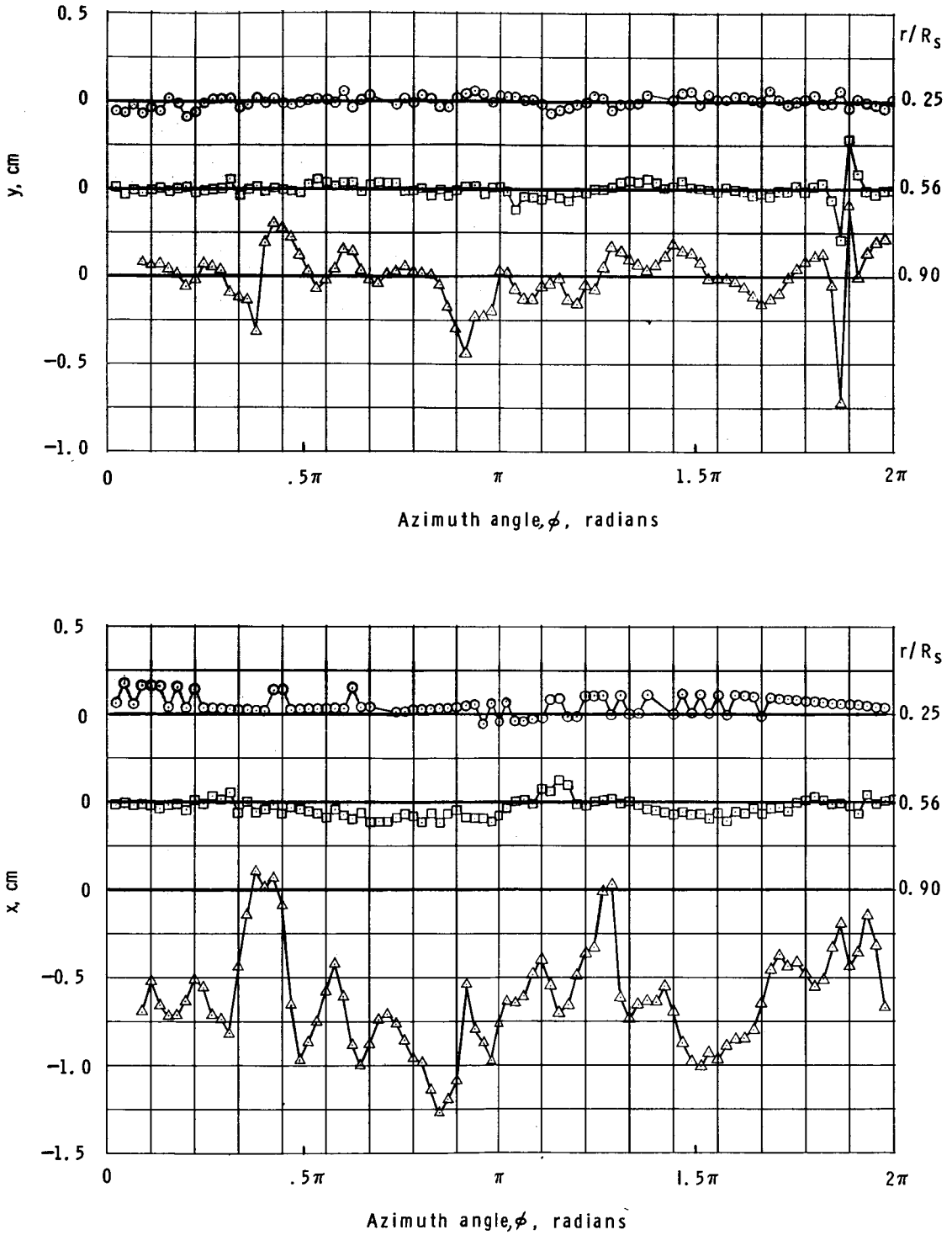

Figure 7.- Image locations at three test radii.

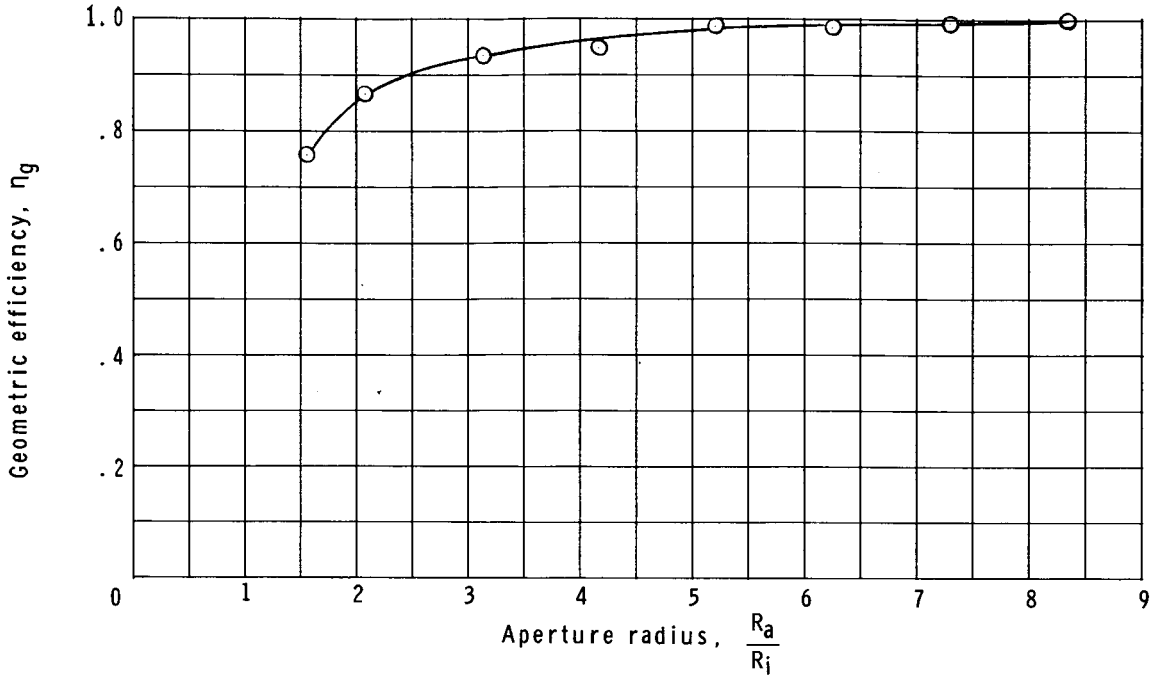

(a) Geometric efficiency. Calorimetric data.

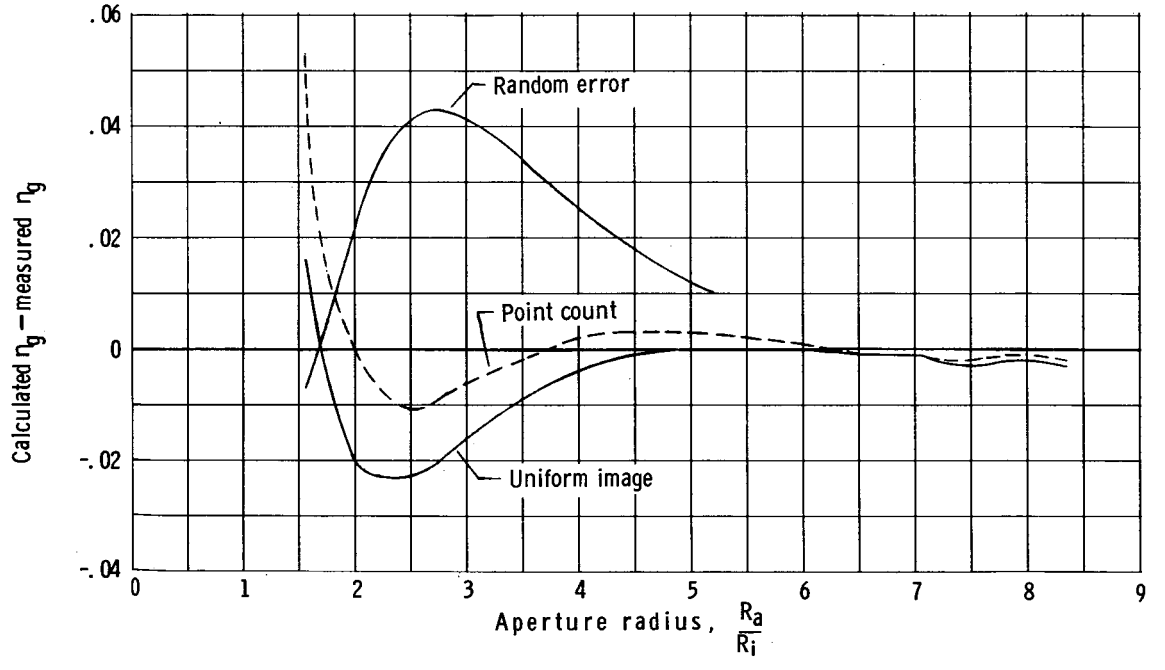

(b) Comparison of accuracy obtained by various methods of calculation.

Figure 8.- Comparison of calculated geometric efficiency with data from calorimetric tests.

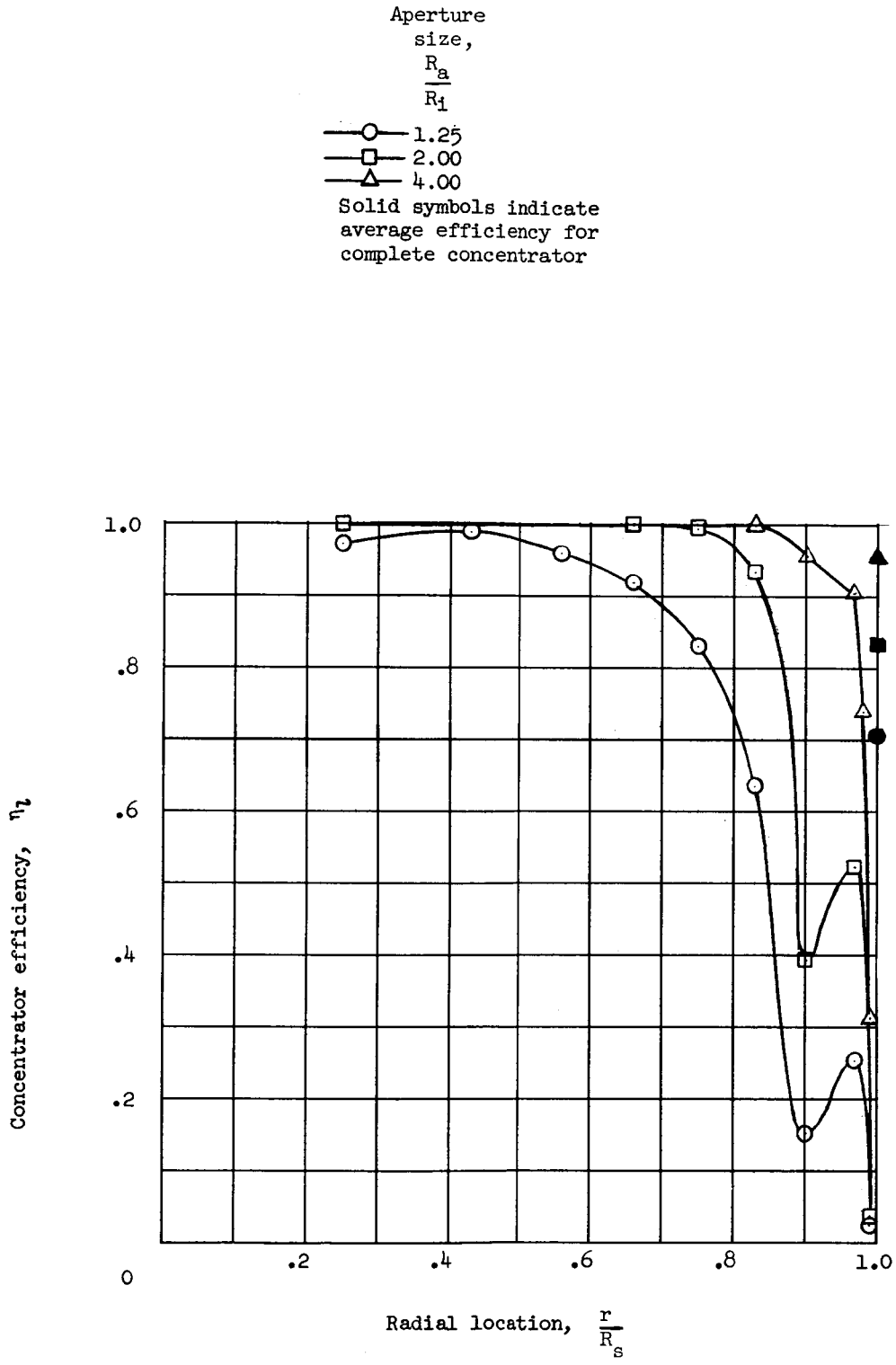

Figure 9.- Variation in local efficiency with concentrator radius, calculated by uniform-image method.

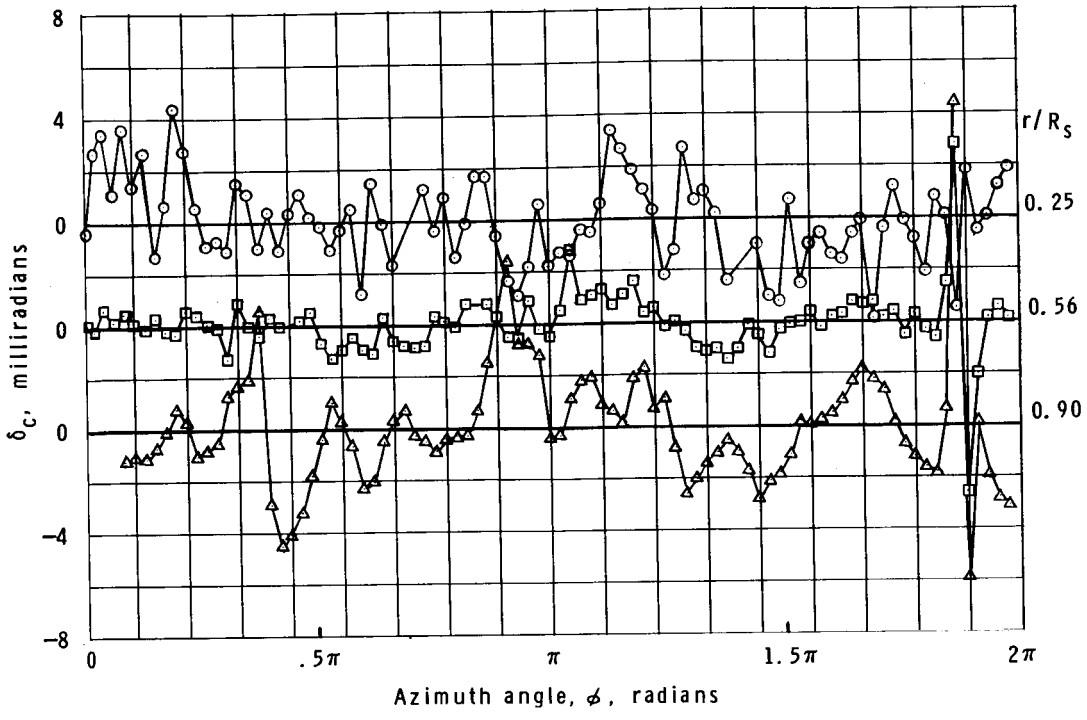

(a) Circumferential error.

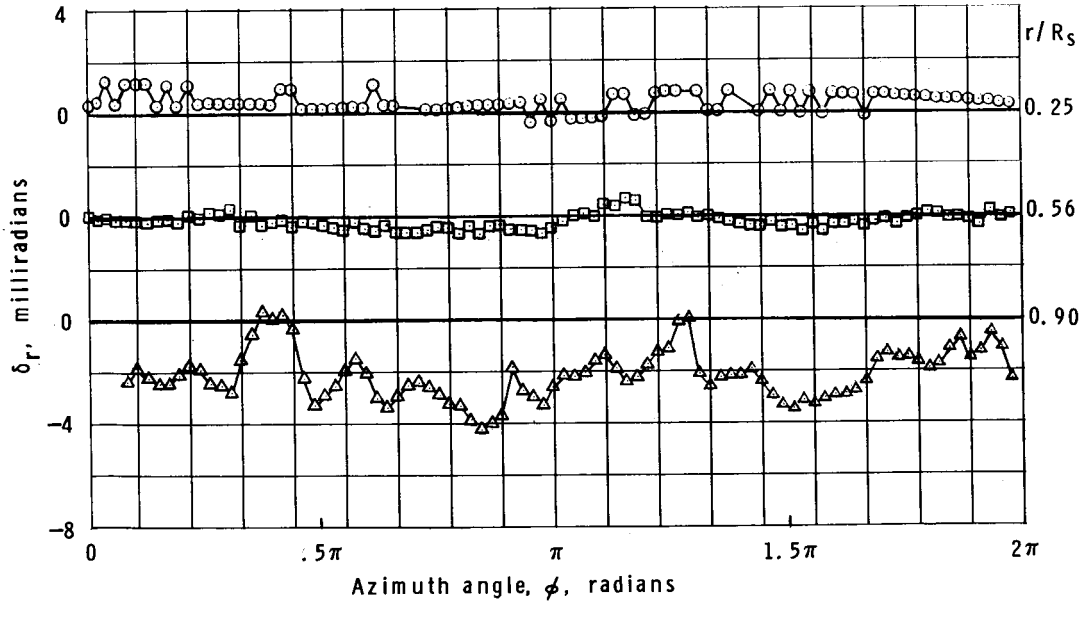

(b) Radial error.

Figure 10.- Concentrator surface slope errors.

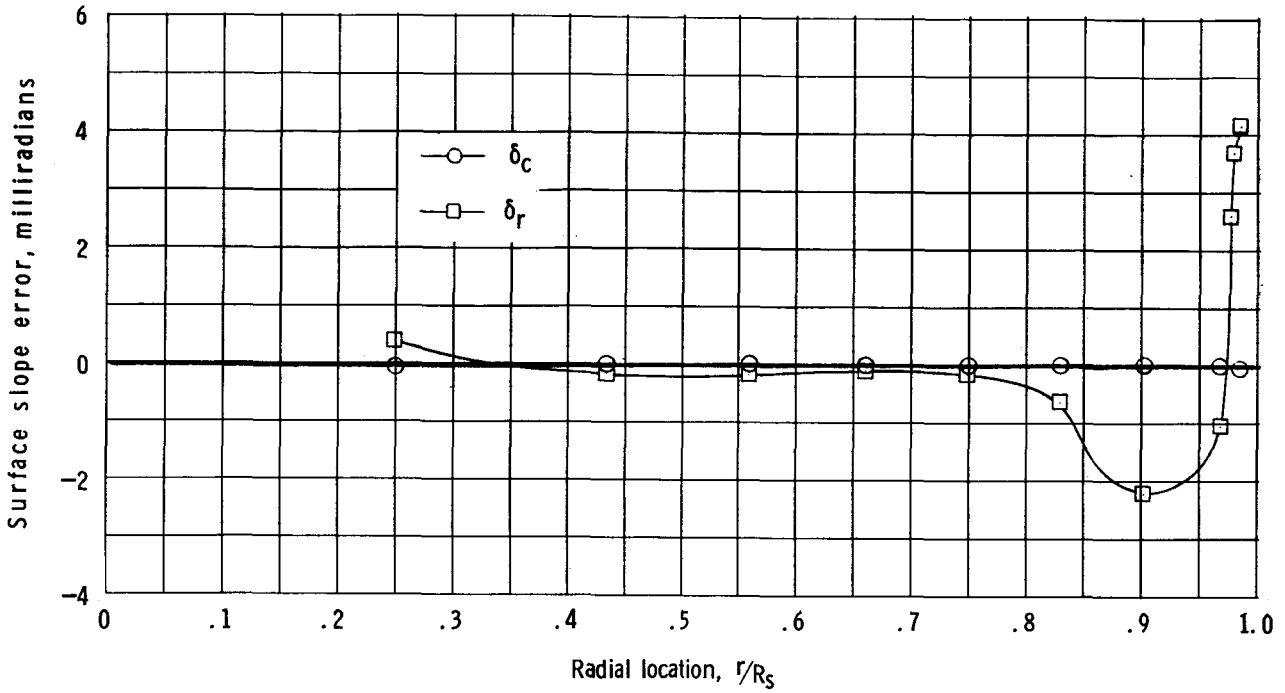

(a) Average local error.

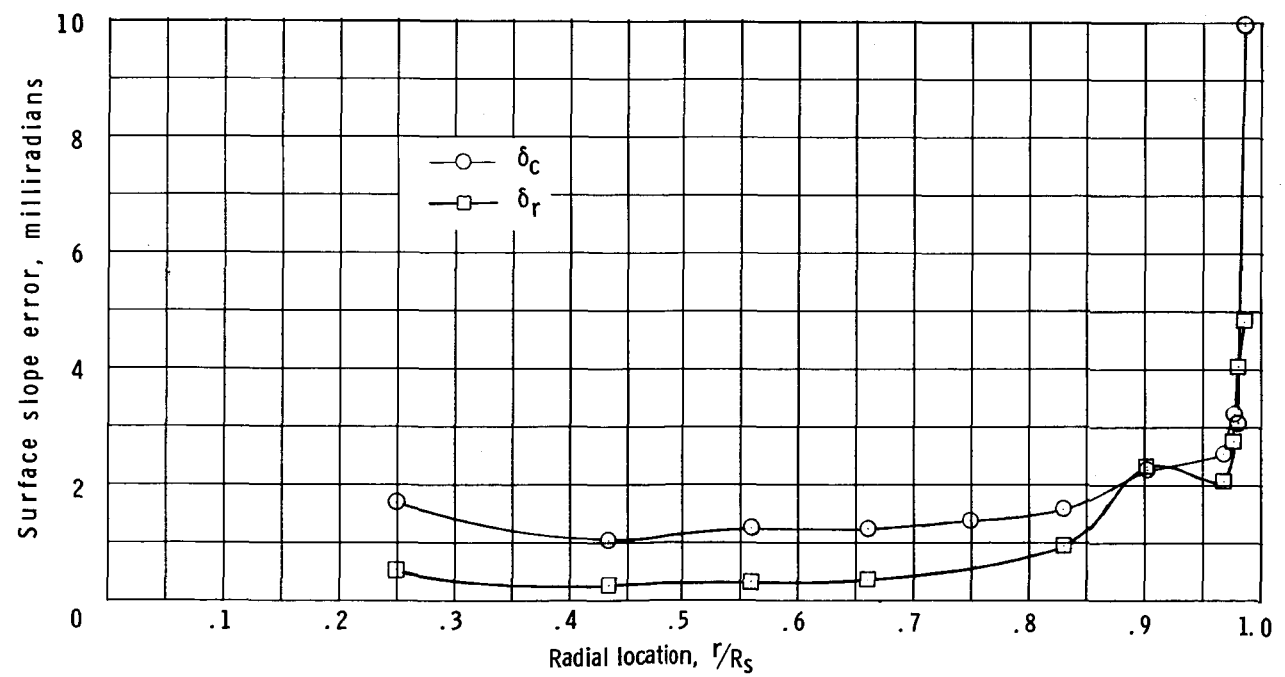

(b) Root-mean-square local error.

Figure 11.- Variation in surface slope error with radial location.

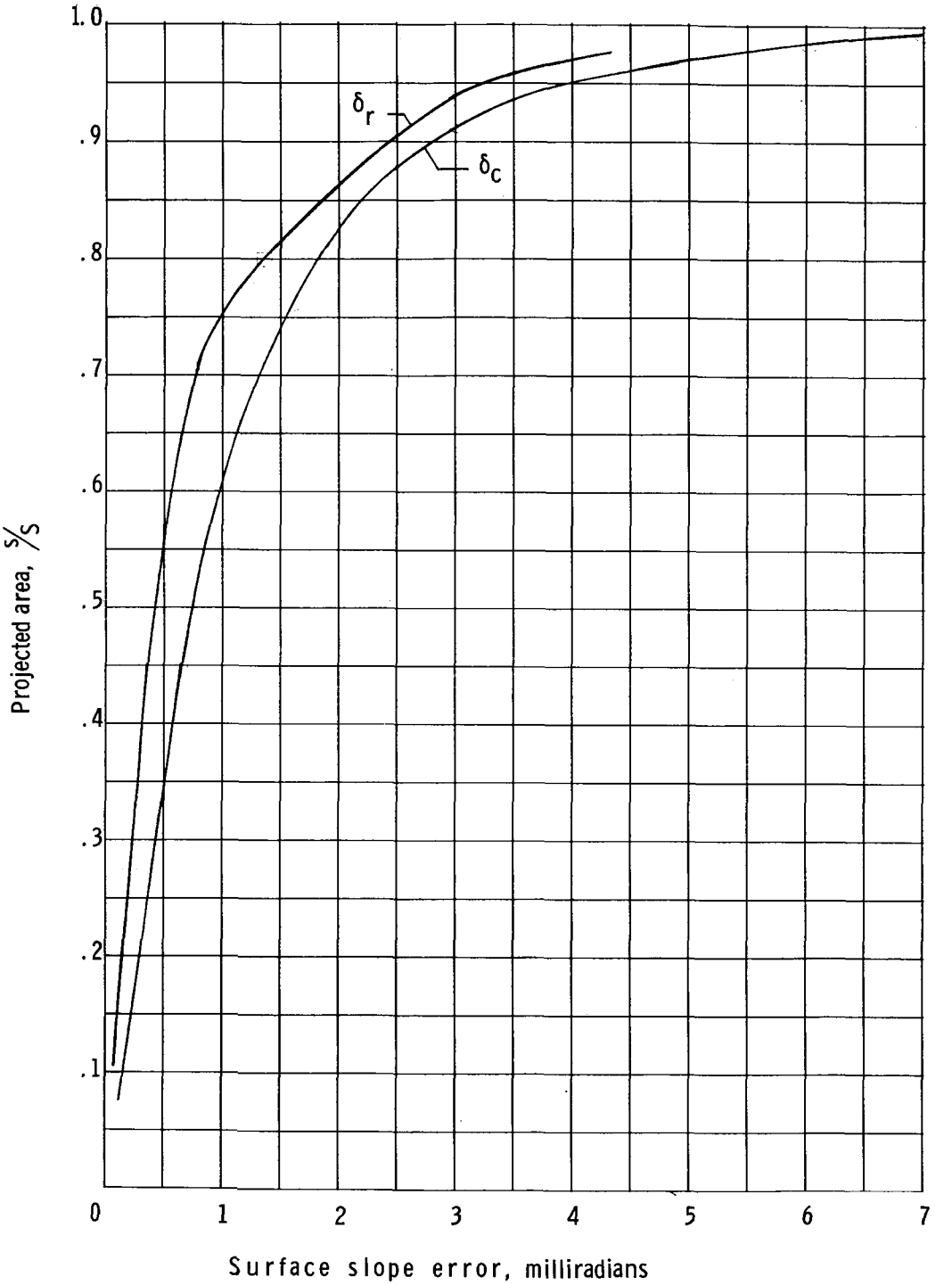

Figure 12.- Fraction of concentrator area having slope errors that are less than a specified value.

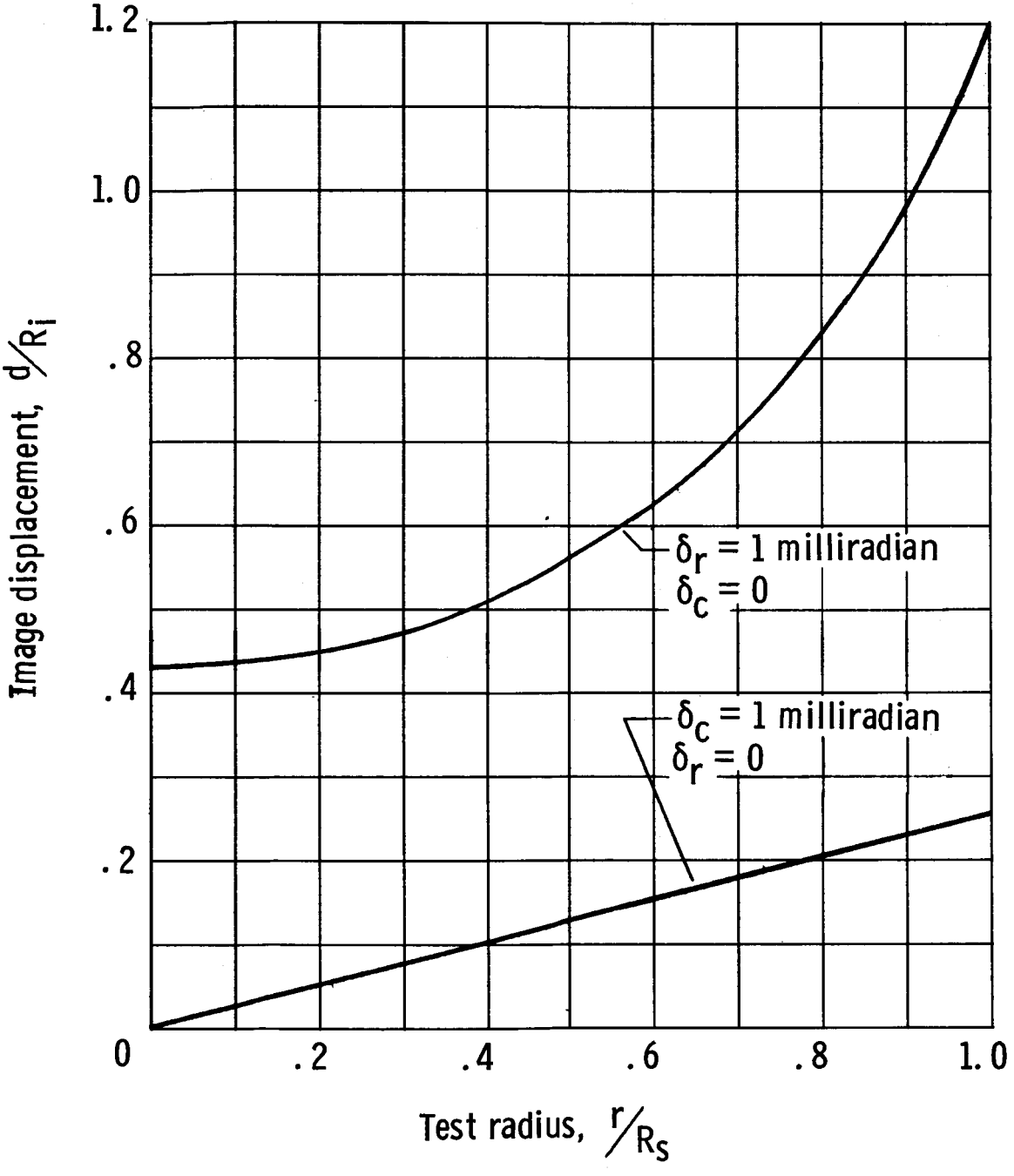

Figure 13.- Variation in image displacement with distance from optical axis for concentrator with f/D = 0.43 and slope error of 1 milliradian.

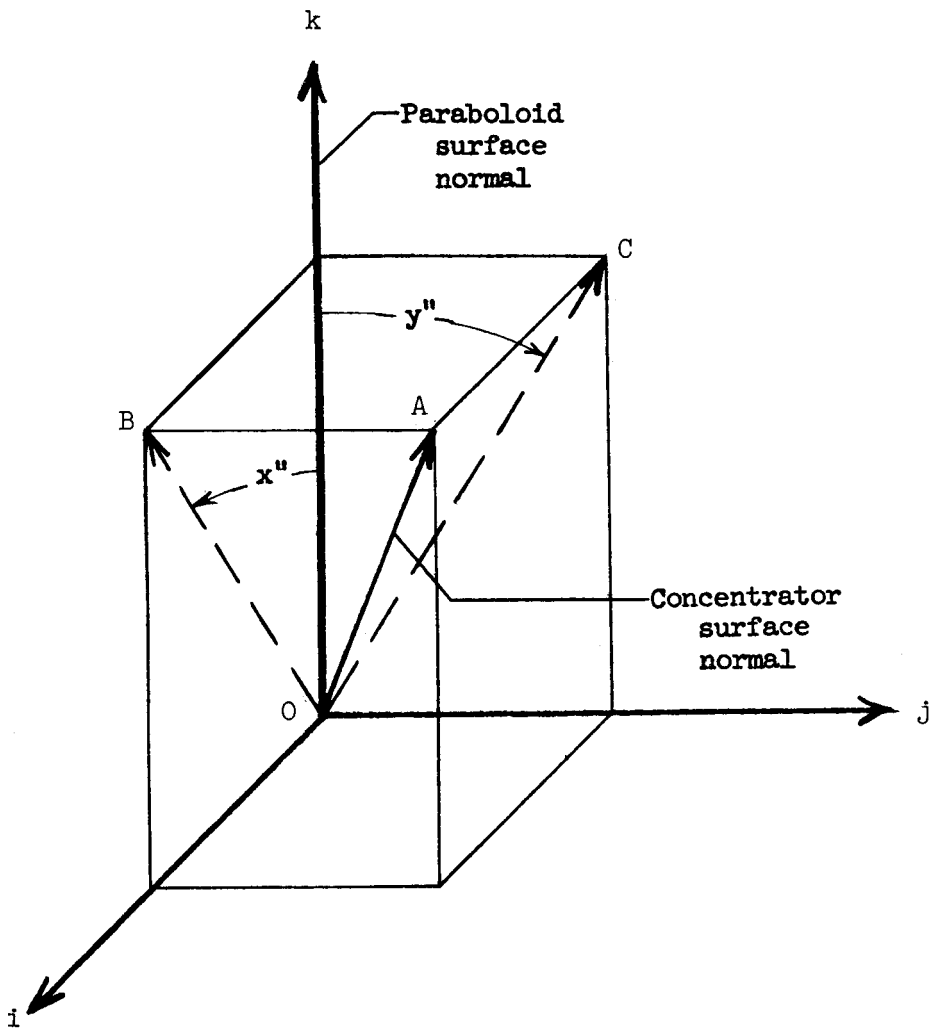

Figure 14.- Sketch defining projected-normal system of slope-error angles.

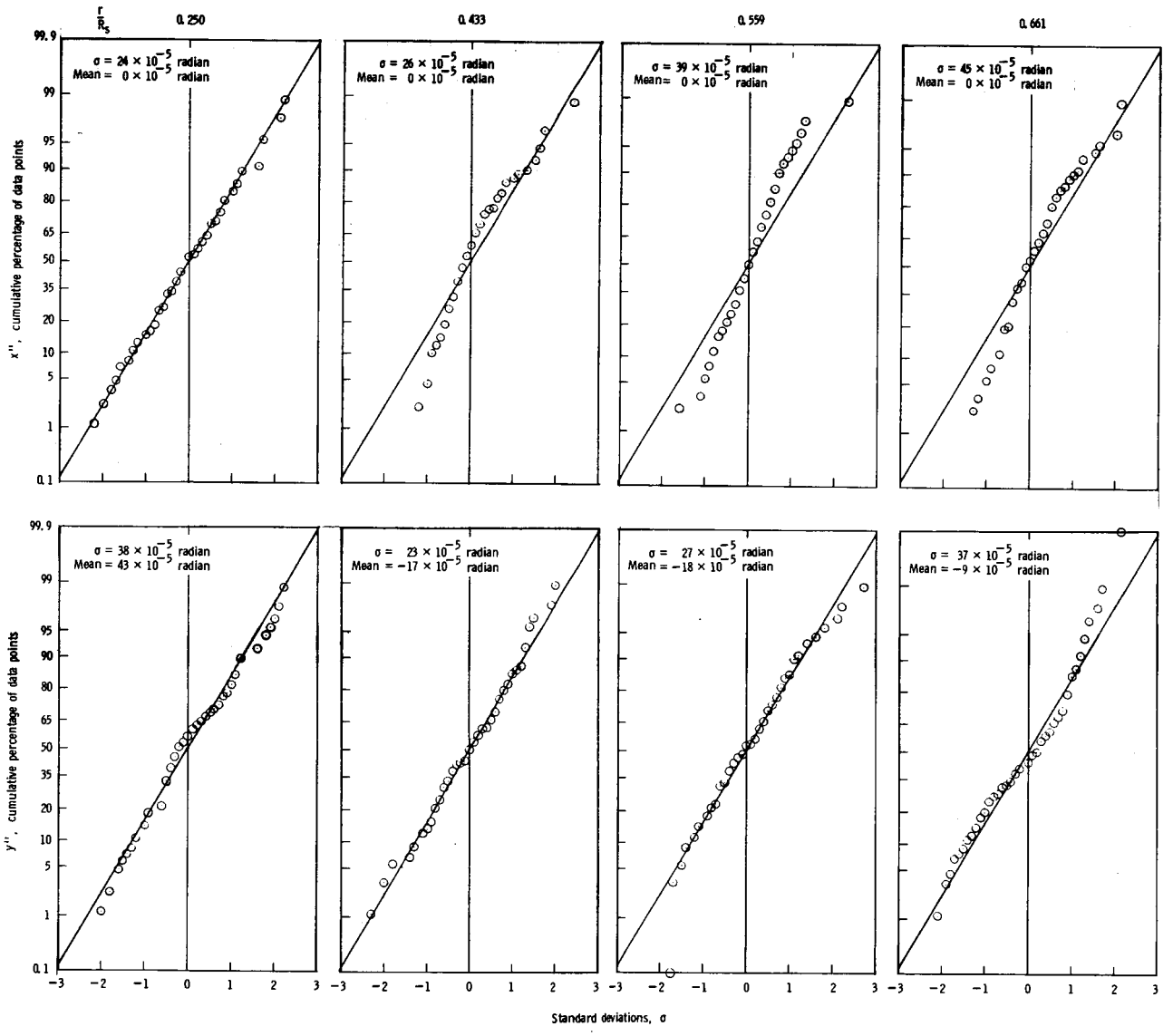

(a) r/R_S = 0.250 to 0.661.

Figure 15.- Comparison of projected-normal slope errors with random distribution (represented by straight line) at each radius.

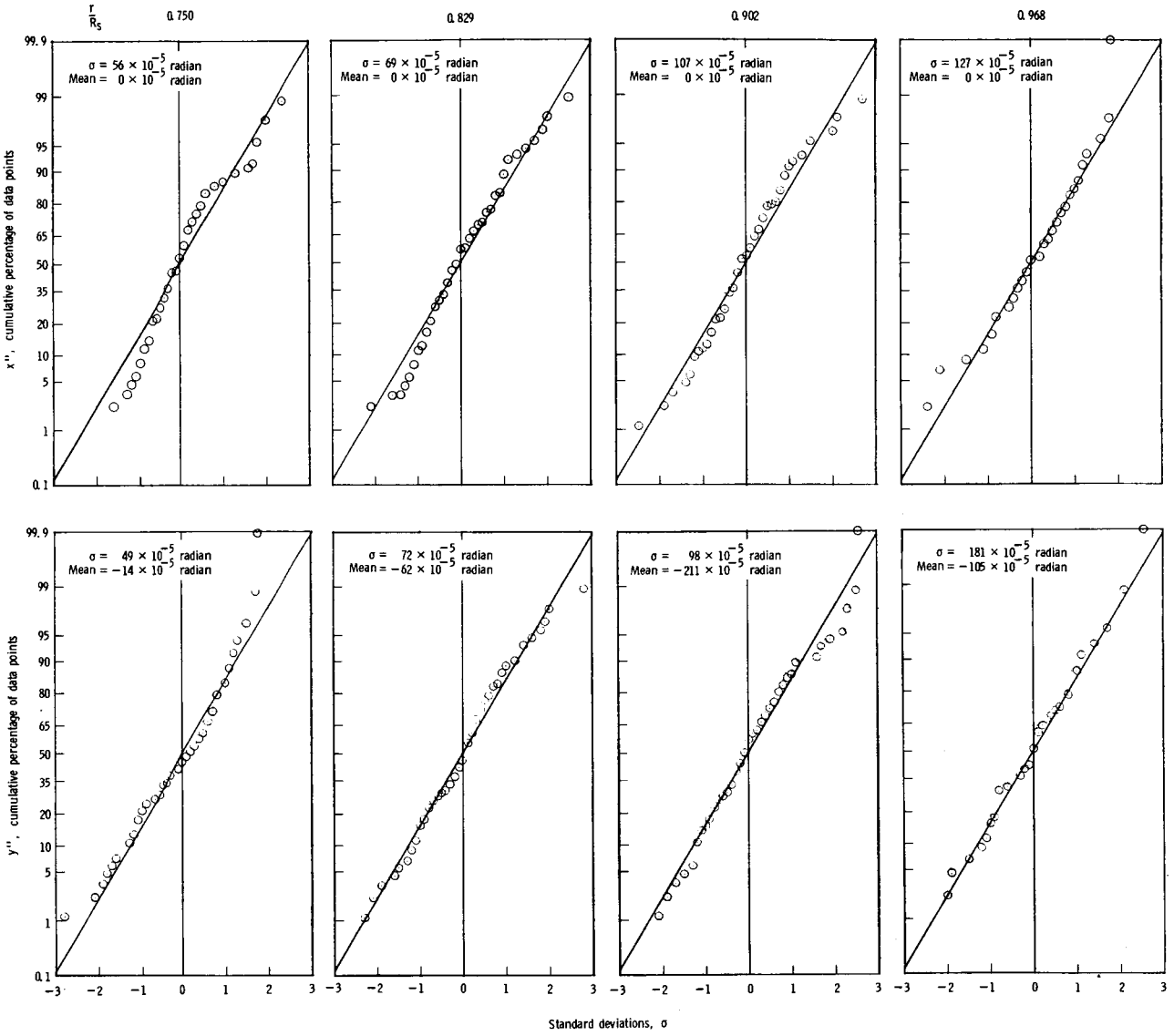

(b) r/R_S = 0.750 to 0.968.

Figure 15.- Concluded.

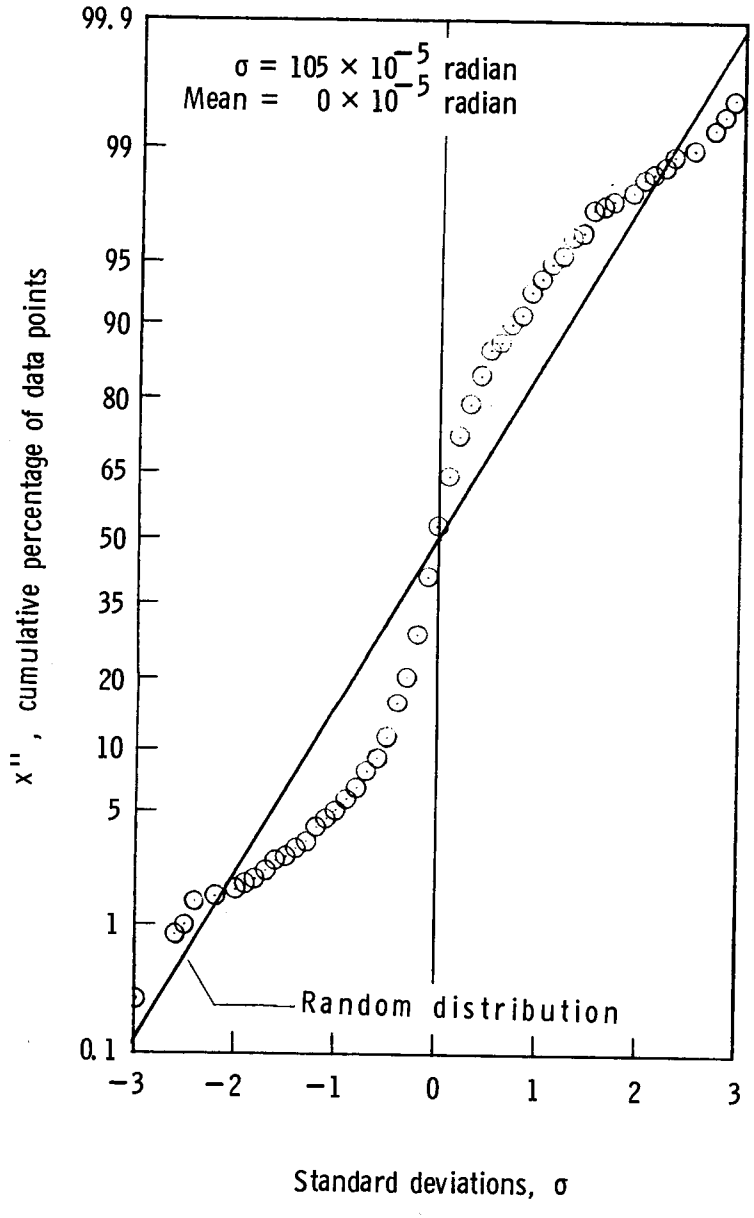

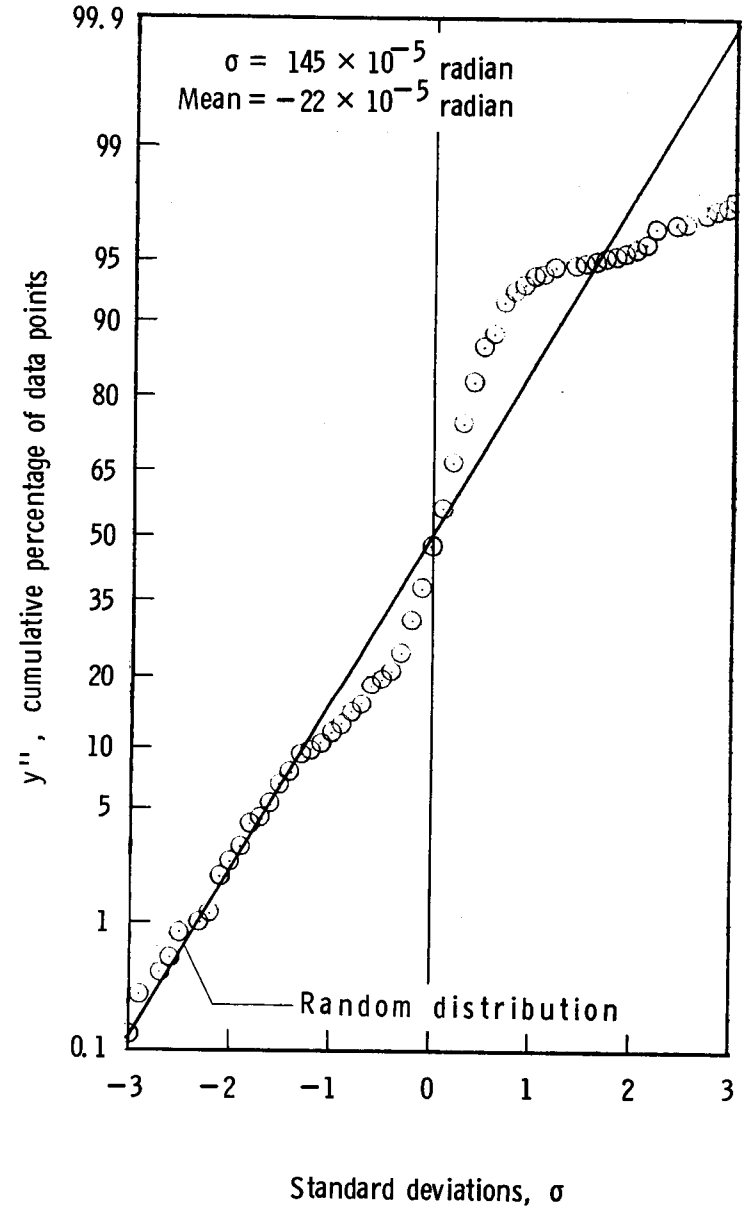

Figure 16.- Comparison of projected-normal slope errors with random distribution. Data for complete concentrator.